A dynamic and prognostic interplay between KSR1, p53 and BRCA1 in breast cancer

Justin Stebbing[1$], Hua Zhang[1$], Aleksandra Filipovic[1], Ylenia Lombardo[1], Arnhild Grothey[1], Lei Cheng Lit[1], Yichen Xu[1], Manikandan Periyasamy[1], Andrew R Green[2], Dongyun Yang[3], Wu Zhang[3], R Charles Coombes[1], Ian O Ellis[2], Heinz-Josef Lenz[3] and Georgios Giamas[1*]

[1]Department of Surgery and Cancer, Division of Cancer, Imperial College London, Hammersmith Hospital Campus, Du Cane Road, London, W12 ONN, UK

[2]Department of Cellular Pathology, Queen's Medical Centre, Nottingham University Hospital NHS Trust, Hucknall Road, Nottingham, NG5 1PB, UK

[3]Division of Medical Oncology, University of Southern California, Norris Comprehensive Cancer Centre, Keck School of Medicine, Los Angeles, CA 90033, USA

Keywords: KSR1, BRCA1, p53, breast cancer, prognosis

[$] These Authors contributed equally to this study.

*To whom correspondence should be addressed:

Dr Georgios Giamas
Imperial College London
Hammersmith Hospital Campus
Du Cane Road
W12 0NN
London, UK
Tel: +44 20 7594 2804
E mail: g.giamas@imperial.ac.uk

Abstract

A human kinome screen identified kinase suppressor of ras-1 (KSR1) as a regulator of estrogen receptor α (ERα) and recent studies suggest that KSR1 may have dual functions as a scaffold protein and as a kinase. Although KSR1 has been implicated in Ras-dependent tumors, its role in breast cancer has not been investigated. In multivariate analyses high KSR1 expression was significantly associated with longer DFS (*p=0.014*) and OS (*p=0.012*). Interestingly, KSR1 was associated positively with BRCA1 (*p=0.002*) and inversely with p53 levels (*p=0.038*). MCF7-KSR1 stable cell line had a significant decreased number of colonies and formed smaller size colonies compared to MCF7-parental cells. Our *in vivo* mouse model demonstrated that xenografts tumor volumes over-expressing KSR1 were significantly reduced compared to controls. SILAC analysis revealed various novel KSR1-regulated proteins and phospho-proteins. Mechanistically, over-expression of KSR1 decreases the transcriptional activity of p53 by reducing the phosphorylation of DBC1, which leads to a reduced interaction of DBC1 with SIRT1 therefore allowing SIRT1 to deacetylate p53. Moreover, KSR1 stabilizes BRCA1 protein levels by up-regulating BARD1 expression and promoting the interaction between BRCA1 and BARD1. Our data link these factors in a continuum with clinical relevance and positions KSR1 in the major oncoprotein pathways in breast tumorigenesis.

Estrogen regulates breast cancer growth through the action of the estrogen receptor alpha (ERα) and therapies targeting this pathway have transformed treatment. Despite this, 1-1.5% of women diagnosed with primary breast cancer subsequently relapse each year, highlighting the need for the discovery of new regulatory targets and mechanisms implicated in this process [1,2]. We have previously performed a short interfering RNA (siRNA) screen and identified a number of protein kinases whose silencing alters the estrogen genomic response in breast cancer cells [3]. Amongst them was kinase suppressor of ras 1 (KSR1), initially described as a novel protein kinase functioning either downstream of RAS or on a parallel pathway to RAF by a genetic screening [4-7]. KSR1, a ceramide-activated proline-directed serine-threonine kinase has been shown to directly phosphorylate and activate Raf-1 but also serves as a scaffold for the Raf-1-mitogen-activated protein kinase (Mek)-extracellular signal-regulated kinase (Erk)-mitogen-activated protein kinase pathway [8-10]. KSR1 has been extensively referred to as a pseudokinase, owing to the fact that there is controversy regarding whether its kinase domain is active, as suggested in one recent study [11], or it serves as a scaffold protein to organize spatiotemporal regulation of the ERK cascade [12], or perhaps both. Such findings add significant complexity to the simple view of ERK pathway control and identify pseudokinases such as KSR1 as potential therapeutic targets.

The function of KSR1 in human disorders has been undefined although KSR1-deficient mice are prone to colitis [13] but on the other hand fail to develop arthritis [14]; it also recruits inducible nitric oxide (NO) synthase and heat shock protein-90 to release NO during pulmonary infection [15]. Previous studies reported that KSR1 regulates the proliferative and oncogenic potential of cells and inhibition of KSR1 abrogates Ras-dependent pancreatic cancer [16,17]. However, as Ras gene mutations are rare in breast cancer, it is similarly unclear whether the role of KSR1 is similar to its role in Ras-dependent cancers [18], and its biologic function in this setting is unexplored, as are its major partner proteins and pathways including those connected to p53 and BRCA1, both of which we implicate here.

The p53 tumor suppressor is well known to play a central role in cell growth arrest, apoptosis and cellular response to genotoxic stress [19,20]. Its transcriptional activity is highly regulated by post-transcriptional modifications including acetylation [21,22]. Previous data showed that deleted in breast cancer 1 (DBC1) directly interacts and negatively regulates the deacetylase SIRT1 resulting in an increase of p53 acetylation [23,24]. Recent evidence describe that phosphorylation of DBC1 is necessary for its interaction with SIRT1 while it inhibits the activity of SIRT1 in response to DNA damage [25,26]. *BRCA1* tumor suppressor gene mutations contribute to a

proportion of hereditary breast and ovarian cancers [27]. BRCA1 forms a heterodimer with the BRCA1-associated ring domain 1 (BARD1) protein, which was discovered in a yeast two-hybrid screen as a binding partner of BRCA1 [28]. Later work suggested that BARD1 stabilises BRCA1 by inhibiting its ubiquitination [29,30].

Herein, we initially evaluated the clinical significance of KSR1 in a large cohort of breast cancer patients and found a significant association of KSR1 with overall and disease free survival. We next established that high KSR1 expression inhibits tumor growth both *in vitro* and *in vivo*.Using SILAC technique we identified novel proteins that are regulated by KSR1 in breast cancer cells. In aggregate, we describe a novel role of KSR1 on the regulation of p53 acetylation and BRCA1 ubiquitination.

Results

KSR1 is an independent predictor of overall survival in breast cancer.

To investigate the clinical significance of KSR1 in breast cancer patients, tissue microarrays (TMAs) containing > 1000 primary operable breast cancer cases from the previously validated Nottingham Tenovus Primary Breast Carcinoma Series were employed. Cytoplasmic KSR1 abundance in breast cancer tissues was determined by immunohistochemistry in accordance to its expression levels (**Figure 1a**). High KSR1 levels were significantly associated with longer overall survival (p = 0.012; **Figure 1b**) and an increased disease free survival (p = 0.014; **Figure 1c**) in a 240 months follow-up. KSR1 was not predictive of response to endocrine therapy (p = 0.064; **Figure 1d**) or adjuvant chemotherapy (p = 0.096; **Figure 1e**). In addition, no significant association of KSR1 with main breast cancer biomarkers was observed (**Table 1**). However, high KSR1 was associated with high BRCA1 (p = 0.002; **table 1**) and low p53 levels (p = 0.038; **table 1**). Multivariate Cox-proportional hazards analysis revealed KSR1 as an independent prognostic factor (**table 2**). We also identified two intronic KSR1 polymorphisms (*rs2241906* and *rs1075952*) but they were not correlated with either disease free or overall survival (**Figure S1**). Finally, we performed an Oncomine [31] analysis of KSR1 gene expression. From 28 analyses based on 11 datasets, there were four[32-35] with a significant p value ($p<0.05$) and gene rank in the top 18% among all differentially expressed genes. In all of these cases, KSR1 was consistently up-regulated in normal breast tissue compared to invasive cancers (**Figure S2**).

KSR1 over-expression inhibits tumor formation and growth *in vitro* and *in vivo*.

Based on the significance of KSR1 in primary breast cancer, we decided to take a 'bedside to bench' approach and examine the role of KSR1 *in vitro*. Analysis of the gene and protein expression levels of KSR1 in a panel of breast cancer cell lines showed that KSR1 is ubiquitously expressed at various levels (**Figure S3**). In accordance with our clinical cohort observation (**table 1**) there was no association between the expression levels of KSR1 and ERα status.

Following, we investigated the role of KSR1 in growth and colony formation of breast cancer cells. For this reason, we generated an MCF7 cell line stably over-expressing KSR1 (MCF7-KSR1; **Figure S4**) and performed a 3D Matrigel-overlay assay, which allows integration of the extracellular matrix signalling components. Over-expression of KSR1 significantly reduced the size of the large and loose aggregates formed by the MCF7 parental cells (**Figure 2a**). Similar

results were observed in the soft agar assay, where the total number and size of cell colonies was analyzed. MCF7-KSR1 cells derived a significantly lesser number of smaller colonies compared to MCF7 parental cells (**Figure 2b,** $p < 0.001$).

We also explored the effects of KSR1 over-expression on tumor growth *in vivo* after subcutaneous transplantation of MCF7-KSR1 (or MCF7-parental cells) into nude mice. The tumour volumes of breast cancer xenografts over-expressing KSR1 were markedly reduced compared with the control group (**Figure 2c**). Immunohistochemical analyses of tumor tissues showed that the Ki67 proliferation index was strongly decreased in MCF7-KSR1 mice showing abundant KSR1 expression (**Figure 2d**).Collectively, both our *in vitro* and *in vivo* results demonstrate the anti-proliferative role of KSR1 further validating its pro-survival contribution in breast cancer patients.

Identification of KSR1-regulated proteins using SILAC.

KSR1 has been extensively referred to as a pseudokinase, since there is controversy regarding whether its kinase domain is active [11] or instead if it serves as a scaffold protein [12] or even perhaps both.

Considering the clinical importance of KSR1 and since its role in breast cancer is poorly understood, we decided to investigate and identify novel proteins (phosphorylated or not) that are differentially regulated by KSR1. For this reason, we performed a quantitative proteomic analysis by stable isotope labelling of amino acids in cell culture. MCF7 cells were grown for 7 cell divisions in either R0K0 'light' medium, containing unlabelled [$^{12}C_6$,$^{14}N_4$]-arginine (Arg) and [$^{12}C_6$]-lysine (Lys) amino acids, or in R10K8 'heavy' medium, containing labelled [$^{13}C_6$,$^{15}N_4$]-Arg and [$^{13}C_6$]-Lys. Following, R0K0 and R10K8 labelled cells were transfected with either empty vector (pCMV6, control) or with a plasmid encoding for full length KSR1 (pCMV6-KSR1), respectively. After 24h, total protein extracts were prepared, mixed 1:1, digested, fractionated, subjected to LC-MS/MS and analysed using MaxQuant [36] (**Figure S5**).

A total of 2504 proteins were identified with either 1 peptide (n_1=424) or a minimum of 2 peptides ($n\geq_2$=2080), both with a false discovery rate of 1%. Out of these proteins, 2032 were quantified (≥1 peptide) and their distribution according to fold changes was determined (**Figure 3a**). Gene ontology classification according to biological and molecular functions, and STRING analysis to identify networks associated with increased or decreased KSR1-regulated proteins was performed, using a cut-off of $\log_2$ ratio >0.5 or <-0.5, (**Tables S1 and S2** and **Figures S6**

and S7).A significance B (Sig B) p-value [36]was calculated in order to identify significant outliers (proteins) from the background population (**Figure 3b and Table S3**).

In order to validate the SILAC proteomic results, we performed Western blotting on selected proteins that were significantly modulated (up or down) after KSR1 over-expression (**Fig 3c**).
We also performed an analysis to identify changes in the phosphorylation status of proteins after KSR1 overexpression; a total of 1407 phosphopeptides were identified out of which, 1165 were quantified (**Tables S4 and S5**; cut-off of $\log_2$ ratio >0.15 or <-0.15). Values from the two independent experiments (total and phosphorylated proteins) were plotted to create a graph showing the $\log_2$ normalised 'total proteins' versus the $\log_2$ 'phosphorylated proteins' ratios (**Figure 3d**). Detailed information for each identified protein, including protein ID's, number of peptides used for identification and their sequence and % coverage, normalised fold changes and $\log_2$ ratios are listed in **Excel file S1**.

KSR1 decreases p53 acetylation by reducing phosphorylation of DBC1 resulting in impaired interaction between DBC1 and SIRT1.

Taking into consideration our clinical data demonstrating a link between KSR1 and p53 / BRCA1 expression, we decided to focus our work on clarifying the connection of KSR1 with these two *bona fide* tumor suppressors. We firstly assessed the effects of KSR1 on p53 transcriptional activity by performing luciferase reporter assays using various p53-dependent gene promoter constructs (including p53-R2, p53-AIP1, p53-IGFBP3 and p53-CYCLIN G1). MCF7 cells were co-transfected with either pCMV6 or pCMV6-KSR1plasmids and each individual p53-dependent promoter construct, in the presence or absence of etoposide, which can induce p53 activity. Interestingly, the luciferase activity of all four different p53-regulated genes was significantly repressed after over-expression of KSR1 (basal levels and after etoposide treatment; **Figure 4a**).
In order to investigate the potential mechanism resulting in the down-regulation of p53 transcriptional activity, we initially evaluated the p53 gene and protein expression after KSR1 over-expression. RT-qPCR and western blotting analyses did not reveal any changes in the p53 mRNA and protein levels respectively after KSR1 over-expression in MCF7 cells (**Figure 4b**). Since the nuclear localisation of p53 is essential for its activity, we examined whether KSR1 could affect p53 compartmentalisation. Immunofluorescence analysis and subcellular protein fractionation did not reveal any cytoplasmic translocation of p53 upon KSR1 over-expression (**Figure 4b**). Moreover, it has been recently reported that neddylation of p53 can inhibit its

transcriptional activity [37,38]. However, our neddylation assay did not show any significant changes following KSR1 over-expression ruling neddylation as the reason for the observed p53 decreased activity (**Figure S8**).

Post-translational modifications of p53 such as phosphorylation and acetylation are essential for p53 activity in response to genotoxic stress [21,22]. Therefore, to examine effects of KSR1 on phospho-p53 and acetylated-p53, MCF7 cells were transfected with pCMV6 or pCMV6-KSR1 plasmids in the presence of etoposide or doxorubicin. While the phosphorylation levels of p53 (Ser15) did not change, interestingly the acetylated-p53 was reduced after KSR1 over-expression upon either etoposide (**Figure 4c**) or doxorubicin (**Figure S9a**) treatment. Moreover, KSR1 silencing rescued the abolished acetylation of p53 after etoposide treatment (**Figure 4d**). Similar results were confirmed in several other cancer cell lines (including ZR75-1, SKBR3 and HCT116; **Figure S9b**).

Total protein levels of SIRT1, which is linked to de-acetylation of p53 [31] were not affected by KSR1 up-regulation (**Figure 4c**). However, according to our SILAC data, amongst the most significantly KSR1-regulated phosphorylated proteins, was 'deleted in breast cancer 1' (DBC1), whose involvement in the regulation of p53 activity and SIRT1 has been previously described [23,24]. Western blotting analysis of DBC1 at Thr454 revealed a decrease in the phosphorylation levels in basal and etoposide-induced conditions (**Figure 4c**). Consistently, knock-down of KSR1 did not alter the total proteins of SIRT1 and DBC1, but increased DBC1 phosphorylation at Thr454 (**Figure 4d**).Finally, since phosphorylated DBC1 interacts stronger with SIRT1 inhibiting its ability to de-acetylate p53 [25,26], we tested whether KSR1 affects the stress-induced SIRT1-DBC1 interaction resulting in the downstream effects on p53 activity. As shown in **Figure 4e**, upon etoposide treatment, the interaction between SIRT1 and DBC1 was undermined after KSR1 over-expression in MCF7, supporting our proposed model that KSR1 is able to inhibit DBC1 phosphorylation resulting in less binding to SIRT1 promoting p53 de-acetylation.

KSR1 stabilizes endogenous BRCA1 by specifically reducing BRCA1 ubiquitination.

Based on the positive correlation between KSR1 and BRCA1 expression on our clinical cohort, we assessed the effects of KSR1 on BRCA1 *in vitro*. Over-expression of KSR1 in MCF7 cells increased BRCA1 protein without altering its mRNA levels, while KSR1 silencing resulted in a decrease of BRCA1 protein (**Figure 4f**). Similar effects were observed in ZR75-1 cells (**Figure S8c**).

Since KSR1 appears to regulate BRCA1 at the protein level, we investigated the involvement of KSR1 on BRCA1 ubiquitination. MCF7 cells treated with different proteasome inhibitors (MG115 and MG132) revealed that KSR1 over-expression resulted in abundant BRCA1 protein levels independent of treatment, while there was a decrease in the ubiquitination of BRCA1 upon over-expression of KSR1 (**Figure 4g**). It is already known that BRCA1 forms a heterodimeric complex with BARD1 that promotes its stabilisation by reducing its ubiquitination, Our western blotting results revealed that up-regulation of KSR1 causes an increase of BARD1 protein while KSR1 silencing decreases the expression of BARD1 (**Figure 4h**). Furthermore, immunoprecipitation evidence indicated that the interaction between BRCA1 and BARD1 was strengthened after KSR1 over-expression (**Figure 4h**). Collectively, our data suggest that KSR1 can stabilize BRCA1 protein by enhancing the interaction between BRCA1 and BARD1, which consequently decreases its ubiquitination.

Discussion

KSR1 was first identified more than 15 years ago as a novel protein kinase implicated in the Ras-Raf pathway: defects in KSR1 inhibits activated Ras, without affecting the pathways induced by activated Raf [39,40]. Interestingly, low levels of KSR1 enhance Ras-induced activity, whereas high KSR1 expression can suppress the Ras pathway [16]. Emerging evidence suggest that KSR1 possess dual activity as a scaffold protein and as active kinase phosphorylating Raf-1 and MEK1 [9-11]. Moreover, KSR1 can also form dimers with Raf modulating its activity [41,42]. Considering the role of KSR1 in Ras-Raf-MAPKs signalling, research has focused on investigating the involvement of KSR1 in Ras-dependent cancers, including skin [43], pancreatic[17] and lung carcinomas [44].Its clinical significance and biologic functions in breast cancer have not been examined.

Our previous work identified KSR1 as a prospective regulator of ERα signaling [3]. In this study, we establish a role of KSR1 as an independent prognostic indicator in breast cancer associating it with a better overall and disease free survival in a large patient cohort (n=1000) with >20 years follow-up. This is the first report to demonstrate a protective role for KSR1 in cancer, as thus far it has been linked to tumor growth induction in pancreatic and lung cancer [17], indicative of a contrasting tissue specific mechanism of function in different biologic contexts. In agreement with our clinical observations, Oncomine analysis revealed that KSR1 gene expression is reduced in different breast cancer dataset, while as expected is up-regulated in lung and colorectal cancers partly due to abnormally activated/mutated Ras signalling pathway.

Following a novel 'bedside to bench' approach, we investigated the biological role of KSR1 *in vitro* and *in vivo*. The physiologically relevant 3D-Matrigel overlay assay, which integrates signals from the extracellular matrix was performed, showing a decrease in the number and size of acini structures formed by KSR1 over-expressing MCF7 cells. To further address the effect of KSR1 on the tumorigenic potential of breast cancer cells, we performed a soft agar assay, where KSR1-MCF7 cells colony formation was significantly compromised. Moreover, results from breast cancer mice xenografts revealed that KSR1 abundance markedly inhibits tumor growth, further supporting the positive clinical significance of KSR1. We also identified novel KSR1-regulated proteins and signalling networks that KSR1 is involved in, apart from the classical Ras-Raf-MAPKs pathway, by performing a SILAC experiment. The observation that KSR1 expression is associated with low p53 and high BRCA1 in breast cancer tissues was further investigated. Interestingly, KSR1 over-expression suppressed p53 transcriptional activity

by reducing the acetylation of p53, while silencing of KSR1 had the opposite effects. It is already known that SIRT1 is able to deacetylate p53 [22,45] while DBC1 can interact with and negatively regulate SIRT1 resulting in increased p53 acetylation [23,24]. Moreover, phosphorylation of DBC1, induced by genotoxic stress, enhances the interaction between SIRT1 and DBC1 [25,26]. Our SILAC data and further *in vitro* experiments using a number of relevant cell lines (MCF7, ZR75-1, SKBR3 and HCT116), demonstrated that KSR1 over-expression decreases the phosphorylation of DBC1, attenuating the interaction of SIRT1-DBC1 leading to declined p53 acetylation.

The correlation between KSR1 and BRCA1 in breast cancer tissues pinpoints the potential role of KSR1 in tumor suppression. Our *in vitro* results showing increased BRCA1 levels after KSR1 over-expression are in accordance with the clinical findings. We also determined that KSR1 increases BARD1 protein, which has been previously reported to form a heterodimer with BRCA1 thereby stabilising it by reducing its ubiquitination [29]. Moreover, KSR1 over-expression enhanced the interaction between BRCA1 and BARD1, which is important for tumor inhibition in breast cancer as previously described [28].

Taken together, we propose a model (**Figure 5**) where KSR1 is implicated in a dynamic interplay involving p53 and BRCA1 and present *in vitro*, *in vivo* and clinical evidence that indicate the tumor suppressor functions of KSR1 and its prognostic significance in breast cancer. Since the role of KSR1 as a kinase and/or as a scaffold protein still remains controversial, further investigation is needed to elucidate which of these features are required for the observed results presented herein. Finally, the identification of novel KSR1-regulated proteins will shed light on new KSR1-modulated signalling pathways implicated in breast cancer.

Acknowledgements

We would like to thank Chun Fui Lai, Monica Faronato and Ombretta Melaiu for their technical assistance and Pritesh Trivedi for performing the immunohistochemistry staining. This work was supported by the Imperial Biomedical Research Centre, the Experimental Cancer Medicine Centre, the National Institute for Health Research and Cancer Research UK. We thank Richard and Evelina Girling and the 'kinase group' for their support.

Author contributions

H.Z., J.S. and G.G. conceived of the study, initiated, designed, supervised and conducted most of the experiments and wrote the manuscript. H.Z., J.S., R.C.C, H.J.L. and G.G. contributed to manuscript editing. H.Z., A.F., Y.L., M.P., A.G., LC.L., Y.X., W.Z., performed *in vitro* and *in vivo* experiments (including quantitative RT-PCR, soft agar and 3D matrigel assays, mouse xenograft model). A.F., H.Z. and J.S. performed the immunohistochemistry scoring. D.Y., W.Z. and H.J.L. generated the single-nucleotide polymorphism data. A.R.G. and I.O.E. performed the statistical analysis of the clinical data. All authors discussed the results, conceived further experiments, commented on the manuscript and approved the final submitted version.

Competing financial interests

The authors declare no competing financial interests.

Figure legends

Figure 1. **Association of KSR1 expression with clinical outcome in breast cancer. a**) Immunohistochemistry staining (IHC) of paraffin embedded breast cancer tissues for KSR1 expression. Representative images of staining intensities: i) negative, ii) 1+, iii) 2+ and iv) 3+. Images were adopted from the high resolution digital imaging (NanoZomer,Hamamatsu Photonics, Welwyn Garden City, UK) with a web-based interface (Distiller, Slide-Path Ltd., Dublin, Ireland) Magnification, x 100. **b**) Kaplan-Meier survival curves for KSR1 expression levels with overall survival (High = 278, Low = 527; $p = 0.012$) and disease free survival (High = 325, Low = 620; $p = 0.012$) in a 240 months follow-up. **c**) Kaplan-Meier overall survival curves for KSR1 expression levels with response to endocrine therapy (High = 101, Low = 171; $p = 0.064$) and to chemotherapy (High = 58, Low = 97; $p = 0.096$) in a 240 months follow-up.

Figure 2. **Effects of stable over-expression of KSR1 on breast cancer tumour growth *in vitro* and *in vivo*. a**) 3-D Matrigel overlay assay. MCF7-parental or MCF7-KSR1 cells were embedded in Matrigel and cultured for 10 days in 10% FCS DMEM supplemented with 2% Matrigel. Phase contrast images of representative acini structures were taken at Day 10. Scale bar, 50 µm. **b**) Soft agar growth assay. MCF7-parental or MCF7-KSR1 cells were incubated for 14 days in soft agar. Optical sections of representative colonies are shown. Scale bar, 50 µm. Colonies from soft agar assay were counted in 5 random fields per well. Diameters of colonies were measured and grouped as (≤75 µm, 75-100 µm and 100 µm). Bar chart shows data of three independent experiments, mean ± SD (*$p<0.001$). **c**) Breast cancer xenograft model in BalbC nude mice. 5×10^6 MCF7-vector or MCF7-KSR1 cells were injected subcutaneously in the flanks of nude mice (n = 8). Tumor volume was measured every 3 days using callipers. Growth curves shown are mean tumour ± SD. Representative set of xenografts derived from MCF7-parental or MCF7-KSR1 cells are shown. **d**) Representative IHC analyses for KSR1 and Ki67 on paraffin-embedded section of xenografts derived from MCF7-parental or MCF7-KSR1 cells.

Figure 3. Protein identification and quantification of KSR1-regulated proteins using SILAC. a) Distribution of 2033 identified KSR1-regulated proteins according to $\log_2$ ratios. **b**) Significance B (Sig B) testing of KSR1-regulated proteins, after examining the ratio and intensity based p-value that indicates the probability that specific proteins are significant outliers from the background population. **c**) **d**) Graph highlighting the outliers within the phospho-peptides data that may be of interest as they do not fall into the general gradient of 1 (indicated by the red line). The ratio's that do fall within this gradient have equivalent regulation levels as their un-

phosphorylated counter-peptides and any differences in regulation are explained by an equivalent regulation in the non-phospho experiment. (The outliers show a different regulation from the non-phospho expt peptides and the treatment they both underwent, indicating there is a genuine increase in phosphorylation stoichiometry within these peptides.)

Figure 4. **Mechanisms of KSR1-regulated p53 transcriptional activity and BRCA1 ubiquitination. a**) E**ffects of KSR1 over-expression on p53 transcriptional activity in the presence or absence of etoposide by luciferase assays.** MCF7 cells were transiently co-transfected with either pCMV6 (vector) or pCMV6-KSR1 plasmids in the presence of four individual p53-dependent promoter constructs expressing firefly luciferase genes (p53-R2, p53-AIP1, p53-CYCLIN G1, and p53-IGFBP3) following DMSO or etoposide (40μM) treatment for 3h. Firefly luciferase activity was measured (renilla luciferase activity was used to normalize transfection efficiency). The normalized luciferase activity of empty vector is set as 1. Results shown are the average of at least three independent experiments and error bars represent SD. **b**) **Effects on mRNA, total protein and subcellular localization of p53 after KSR1 over-expression.** MCF7 cells were transiently transfected with pCMV6 (vector) or pCMV6-KSR1 plasmids for 24 hours. Total mRNA and protein were extracted as described in Materials and Methods. Subsequently, relative mRNA levels of *TP53* and p53 total protein were measured by qRT-PCR and western blotting, respectively. Gene expression level from cells transfected with pCMV6 was set as 1. Results shown are the average of at least three independent experiments and error bars represent SD. Protein fractions from the nucleus and cytoplasm were extracted as described in Materials and Methods. Rb and Tubulin expression served as positive normalising control for nuclear and cytoplasmic proteins respectively. Immunofluorscence staining of p53 in MCF7 cells after 24 hours transfection with either pCMV6 or pCMV6-KSR1 plasmids. p53 was detected with an anti-p53 antibody while the nucleus was stained with DAPI. Representative pictures of three independent experiments are shown. **c**) **Effects on p53 acetylation and phosphorylation of DBC1 after KSR1 over-expression followed by a titration of etoposide treatment.** MCF7 cells were transiently transfected with pCMV6 (vector) or pCMV6-KSR1 plasmids for 24 hours Following, cells were treated with various concentration of etoposide (20, 40, 80 μM, 3h). p53 acetylation and DBC1 phosphorylation at Thr454 were assessed by immunoblotting with specific antibodies as indicated. **d**) **Effects on p53 acetylation and phosphorylation of DBC1 after KSR1 silencing followed by a titration of etoposide treatment.** MCF7 cells were transfected with control siRNA (siCT) or siKSR1 for 72 hours followed by etoposide treatment (20, 40, 80 μM, 3h). p53 acetylation and DBC1

phosphorylation at Thr454 were assessed by immunoblotting with specific antibodies as indicated.) **e**) **Interaction of DBC1 and SIRT1 after KSR1 over-expression with etoposide treatment by immunoprecipitation.** MCF7 cells were transiently transfected with pCMV6 or pCMV6-KSR1 plasmids for 24 hours. Subsequently, cells were treated with etoposide (40μM, 3h). The interactions between SIRT1 and DBC1 were detected by immunoprecipitation (IP) of SIRT1 or DBC1 followed by immunoblotting with DBC1 and SIRT1 antibodies respectively. **f**) **Effects of KSR1 over-expression and silencing on BRCA1 mRNA and protein levels.** MCF7 cells were transiently transfected with pCMV6 or pCMV6-KSR1 plasmids for 24 hours. For knock-down of KSR1, MCF7 cells were transfected with either control siRNA (siCT) or siKSR1 for 72 hours. Total mRNA and protein were extracted as described in Materials and Methods. Subsequently, relative mRNA levels of *BRCA1* gene were measured by qRT-PCR. Gene expression level from cells transfected with pCMV6 was set as 1. Results shown are the average of at least three independent experiments and error bars represent SD. The protein expression levels of BRCA1 was assessed by western blotting. **g**) **Effects of KSR1 over-expression on BRCA1 ubiquitination.** MCF7 cells were transiently transfected with pCMV6 or pCMV6-KSR1 plasmids for 24 hours, in the presence or absence of MG115 or MG132 proteasome inhibitor (10 μM, 6h). BRCA1 protein levels were assessed by immunoblotting with specific antibodies as indicated. Ubiquitination of BRCA1 was detected by immunoprecipitation of BRCA1 followed by immunoblotting with ubiquitin antibody. **h**) **Effects of KSR1 over-expression on BARD1 protein levels and the interaction between BRCA1 and BARD1**. MCF7 cells were transiently transfected with pCMV6 or pCMV6-KSR1 plasmids for 24 hours. For knock-down of KSR1, MCF7 cells were transfected with either control siRNA (siCT) or siKSR1 for 72 hours. The protein expression levels of BARD1 were assessed by western blotting. The interactions between BRCA1 and BARD1 were detected by immunoprecipitation (IP) of BRCA1 followed by immunoblotting with BARD1 antibody.
All blots shown are representatives of at least three independent experiments (* p<0.05; ** p<0.01; *** p<0.001).

Figure 5 Schematic illustration of a dynamic interplay between KSR1, p53 and BRCA1 in breast cancer. A novel model indicating the role of KSR1 on p53 and BRCA1 is proposed here: **a**) KSR1 reduces DBC1 phosphorylation resulting in a decreased interaction of DBC1 with SIRT allowing SIRT1 to deacetylate p53, which leads to a down-regulation of p53 transcriptional activity. **b**) KSR1 stabilizes BRCA1 protein by increasing BARD1 protein levels enhancing the interaction between BRCA1 and BARD1, which in turn decreases ubiquitination of BRCA1.

Supplementary Figure legends

Figure S1 Correlations of KSR1 polymorphisms with overall survival and disease free survival in breast cancer patients. Kaplan-Meier curves demonstrate the association between two KSR1 polymorphisms: **a**) rs2241906 and **b**) rs1075952 and overall survival ($p1 = 0.3841$; $p2 = 0.4710$) and disease-free survival ($p1 = 0.2481$; $p2 = 0.3529$).

Figure S2 Oncomine data-mining analysis of KSR1 mRNA in breast cancer. Comparison of KSR1 mRNA expression between normal breast tissue versus invasive ductal breast carcinoma in 4 different datasets.

Figure S3 Expressions of KSR1 gene and protein levels in various breast cancer cell lines. a) KSR1 mRNA levels were measured by qRT-PCR. KSR1 expression in MCF7 is set as 1 and all other seven cell lines are normalized relative to MCF7 mRNA levels. Error bars represent SD of 3 experiments, each in triplicate. **b**) Representative western blotting of KSR1 expression is shown. Experiments were repeated at least three times.

Figure S4 Validation of KSR1 stable over-expression breast cancer cell line. MCF7-KSR1 and MCF7-parental stable cells were generated by transfection of either pCMV6-KSR1 or pCMV6-vector into MCF7 cells and selected in the presence of G418 (1 mg/ml). KSR1 overexpression was confirmed by RT-qPCR and western blotting. Results shown are the average of three independent experiments and error bars represent SD of 3 experiments, each in triplicate.

Figure S5 SILAC proteomics workflow. Experimental schematic outline of SILAC experiment.

Figure S6 Classification of KSR1-regulated proteins. Distribution of differentially expressed proteins (cut-off of $\log_2$ ratio >0.5 or <-0.5) after KSR1 overexpression according to their **(a)** biological functions, **(b)** molecular processes and **(c)** cellular compartmentalisation ($p < 0.005$).

Figure S7 Schematic representation of the most significant networks using STRING analysis after KSR1 overexpression. Top networks including the most significantly **(a)** up-regulated and **(b)** down-regulated proteins after KSR1 overexpression in MCF7 cells.

Figure S8 Neddylation assay of p53 after KSR1 over-expression. MCF7 cells were co-transfected with HA-NEDD8 and pCMV6 or pCMV6-KSR1 plasmids as indicated. p53 was immunoprecipitated using a p53 specific antibody (DO-1) and the neddylated-p53 was detected by immunoblotting using anti-NEDD8 and anti-p53 specific antibodies.

Figure S9 Effects of KSR1 over-expression and silencing on either p53 acetylation after doxorubicin treatment, and on BRCA1 protein levels in different cancer cell lines. a) Effects on acetylated p53 after KSR1 over-expression in response to doxorubicin. MCF7 cells were transiently transfected with pCMV6 or pCMV6-KSR1 plasmids for 24 hours, in the presence or absence of doxorubicin. p53 acetylation was assessed by immunoblotting with specific antibody as indicated. **b**) Effects of KSR1 over-expression and knock-down on p53 acetylation in various cancer cell lines. ZR75-1, SKBR3 and HCT116 cells were transiently transfected with pCMV6 or pCMV6-KSR1 plasmids for 24 hours, followed by etoposide treatment. ZR75-1 cells were transfected with control siRNA (siCT) or siKSR1 for 72 hours followed by etoposide treatment. p53 acetylation was assessed by immunoblotting with specific antibody as indicated. **c**) Effects on BRCA1 protein levels after silencing KSR1 in ZR75-1 cells. ZR75-1 cells were transfected with control siRNA (siCT) or siKSR1 for 72 hours and western blotting was performed to assess the expression of BRCA1 using specific antibody.

Materials and methods

Clinical specimens

Tissue microarrays (TMAs) containing > 1000 primary operable breast cancer cases from the previously validated Nottingham Tenovus Primary Breast Carcinoma Series were employed [3,46-48]. This well-characterized resource contains information on patients' clinical and pathological data including histological tumor type, primary tumor size, lymph node status, histological grade and data on other breast cancer relevant biomarkers. These include ERα, PgR, HER2, BRCA1, p53, cytokeratins (CKs; 5/6, 7/8, 18), Ki67 and E-cadherin. The immunoreactivity and scoring were defined in this series as previously described [49]. Patients within the good prognosis group (Nottingham Prognostic Index (NPI) ≤ 3.4) did not receive adjuvant therapy. Hormonal therapy was prescribed to patients with ERα positive tumors and NPI scores > 3.4 (moderate and poor prognostic groups). Pre-menopausal patients within the moderate and poor prognosis groups were candidates for chemotherapy. Conversely, postmenopausal patients with moderate or poor NPI and ERα positive were offered hormonal therapy, while ERα negative patients received chemotherapy. Data collected included overall survival (OS), disease-free survival (DFS). Clinical data were maintained on a prospective basis with a median follow-up was 124 months (range 1 to 233).

Immunohistochenistry

Anti-KSR1 rabbit polyclonal antibody (Santa Cruz, Heidelberg, Germany) was optimized to a working concentration of 2μg on full-face excisional tissue sections. Subsequently, breast cancer TMA (n = 945) cases comprising 4μm thick formalin fixed paraffin embedded tissue cores were immuno-stained with anti-KSR1 on the Leica BOND-MAX automated system using manufacturer's instructions. Hit-induced epitope retrieval was performed in citrate buffer (ER1) for 5 mins. Detection was achieved using the Polymer Detection kit (Leica Microsystems Inc., USA). Determination of the optimal cut-offs were performed using X-tile bioinformatics software (Yale University, USA). Cytoplasmic staining was scored based on intensity ranging from 0 to +3; 0 = null, +1 = low, +2 = intermediate and +3 = high level of staining intensity. Scoring for each tissue core on the TMAs was performed by two independent investigators. High resolution digital imaging (NanoZomer, Hamamatsu Photonics, Welwyn Garden City, UK) at 20x magnification with a web-based interface (Distiller, SlidePath Ltd., Dublin, Ireland) was used. All cases were scored without knowledge of the clinicopathological or outcome data.

Protein digestion and peptide fractionation

Equal amounts of protein from unlabeled and labeled samples were combined prior to protein digestion. Briefly, samples were reduced in 10 mM DTT and alkylated in 50 mM Iodoacetamide prior to boiling in loading buffer, and then separated by one-dimensional SDS-PAGE (4-12% Bis-Tris Novex mini-gel, Invitrogen) and visualized by colloidal Coomassie staining (Novex, Invitrogen). The entire protein gel lanes were excised and cut into 10 slices each. Every gel slice was subjected to in-gel digestion with trypsin overnight at 37 ^{o}C (Lamond et al., 2011). The resulting tryptic peptides were extracted by formic acid (1%) and acetonitile, lyophilized in a speedvac and resuspended in 1% formic acid.

Protein digestion and phosphopeptide enrichment

FASP Procedure was performed as previously described [50]. 500 uL FASP 1 (8 M urea, 20 mM DDT in 100 mM Tris/HCL pH 8.5) was added to ~2 mg protein lysate to dilute SDS concentration and transferred to a Vivacon 500, 30k MWCO HY filter (Sartorius Stedim Biotech, VN01H22). The sample was buffer exchanged using FASP1 several times by spinning the tube at 7000g to remove detergents. The protein lysate was concentrated by centrifugation and diluted in FASP 2 (100 mM Tris/HCl pH 8.5) ready for trypsin digestion. The sample was reduced using 50mM fresh IAA in FASP 2 in the dark for 30mins. Lysates were spun down to remove excess IAA and buffer exchanged into FASP 3 (100mM TEAB (triethyl ammonium bicarbonate)). Trypsin was dissolved in FASP 3 to give a 1:200 enzyme to protein ratio and added in a volume of at least 100 μL for 4-6 hours. This was repeated with fresh trypsin for a further overnight incubation. Lysates were spun down and washed with 0.5M NaCl and 150 μL 10% TFA added to reduce the pH. A standard desalting procedure was used [51].

Hydrophilic Interaction Chromatography (HILIC) fractionation: A TSKgel Amide-80 separation column with a TSKgel Amide guard column was used for HILIC separation of FASP peptides. Buffer A: 80 % ACN, 0.1 % Formic Acid & Buffer B: 0.1 % Formic Acid were used for the gradient at a flow rate of 0.6 mLs/min. The sample was separated into 45 fractions, collected 2mins/vial and dried using a speed vac.

TiO_2 Enrichment was performed as previously described [51]. TiO_2 beads were washed & re-suspended in Buffer B at 50 ug / uL and added to tubes to give 1 mg per tube. The sample was re-suspended in loading buffer, added to beads & incubated at RT for 20 mins. After washes using buffers A & B samples were eluted using aliquots of 0.5% NH_4OH. Elutions were pooled & 10 uL of 20 % FA added to adjust the pH. Samples were dried and re-suspended in 1% FA.

Mass Spectrometry methods

Trypsin-digested peptides were separated using an Ultimate 3000 RSLC (Thermo Scientific) nanoflow LC system. On average 0.5 µg was loaded with a constant flow of 5 µl/min onto an Acclaim PepMap100 nanoViper C18 trap column (100 µm inner-diameter, 2 cm; Themro Scientific). After trap enrichment, peptides were eluted onto an Acclaim PepMap RSLC nanoViper, C18 column (75 µm, 15 cm; Thermo Scientific) with a linear gradient of 2–40% solvent B (80% acetonitrile with 0.08% formic acid) over 65 min with a constant flow of 300 nl/min. The HPLC system was coupled to a linear ion trap Orbitrap hybrid mass spectrometer (LTQ-Orbitrap Velos, Thermo Scientific) via a nano electrospray ion source (Thermo Scientific). The spray voltage was set to 1.2 kV, and the temperature of the heated capillary was set to 250 °C. Full-scan MS survey spectra (*m*/*z* 335–1800) in profile mode were acquired in the Orbitrap with a resolution of 60,000 after accumulation of 1,000,000 ions. The fifteen most intense peptide ions from the preview scan in the Orbitrap were fragmented by collision-induced dissociation (normalized collision energy, 35%; activation Q, 0.250; and activation time, 10 ms) in the LTQ after the accumulation of 10,000 ions. Maximal filling times were 1,000 ms for the full scans and 150 ms for the MS/MS scans. Precursor ion charge state screening was enabled, and all unassigned charge states as well as singly charged species were rejected. The lock mass option was enabled for survey scans to improve mass accuracy (Olsen, J.V. *et al.,* 2004). Data were acquired using the Xcalibur software.

Quantification and bioinformatics analysis

The raw mass spectrometric data files obtained for each experiment were collated into a single quantitated data set using MaxQuant [36] and the Andromeda search engine software [52]. Enzyme specificity was set to that of trypsin, allowing for cleavage N-terminal to proline residues and between aspartic acid and proline residues. Other parameters used were: (i) variable modifications, methionine oxidation, protein N-acetylation, gln → pyro-glu; (ii) fixed modifications, cysteine carbamidomethylation; (iii) database: target-decoy human MaxQuant (ipi.HUMAN.v3.68); (iv) heavy labels: R6K4 and R10K8; (v) MS/MS tolerance: FTMS- 10ppm , ITMS- 0.6 Da; (vi) maximum peptide length, 6; (vii) maximum missed cleavages, 2; (viii) maximum of labeled amino acids, 3; and (ix) false discovery rate, 1%. Peptide ratios were calculated for each arginine- and/or lysine-containing peptide as the peak area of labelled arginine/lysine divided by the peak area of non-labelled arginine/lysine for each single-scan mass spectrum. Peptide ratios for all arginine- and lysine-containing peptides sequenced for

each protein were averaged. Data are normalised using 1/median ratio value for each identified protein group per labelled sample.

In vivo tumorigenicity assay in breast cancer xenografts in nude mice

Female 7-week-old, nu/nu-BALB/c athymic nude mice were acclimated in the animal house one week before experimentation. Before cells injection, a 0.72mg 17-β Estradiol 60-day release pellet was implanted subcutaneously (Innovative Research of America) into each mouse. 5×10^6 MCF7-vector or MCF7-KSR1 cells were resuspended in the total volume of 100μL and were then injected subcutaneously into the flank of the animals by groups (n=9, per group). Tumor growth was analyzed by caliper measurements every three days and calculated using the formula 1/2 [length (mm)] x [width (mm)]^2. After the mice were sacrificed, primary tumors were excised and formalin fixed. Samples were paraffin embedded, cut at 3 μm and IHC stained for histological evaluation of target proteins expression. This study was conducted under the UK Home Office Project License.

Statistical analysis

Statistical analysis for TMAs was performed using SPSS 16.0 statistical software (SPSS Inc., Chicago, IL, USA). Analysis of categorical variables was performed with the appropriate statistical test. Survival curves were analyzed using the Kaplan-Meier method with significance determined by the Log rank test; multivariate analysis was performed by Cox hazards regression analyses. DFS was defined as the period from the date of initial diagnosis to the date of the first documented relapse or death, and OS was defined as the time from the initial diagnosis to death. DFS time was censored at the date of last follow-up if patients were still relapse-free and alive, and OS was censored at the time when patients were alive. A forward stepwise Cox regression model was conducted to select baseline patient demographic and tumor characteristics to be included in the multivariate analyses of 2 KSR1 polymorphisms and clinical outcome. Chi-square tests were used to examine the associations between tumor characteristics and KSR1 polymorphisms. Tests were 2-sided at a 0.05 significance level.

Supplementary Materials and methods

Cell lines, reagents, antibodies and plasmids

MCF7, BT474, T47D, ZR75-1, MDA231, MDA468 and SKBR3 cells were maintained in Dulbecco's Modified Eagle's Medium (DMEM) supplemented with 10% fetal calf serum (FCS) and 1% penicillin (P) / streptomycin (S) / glutamine (G). MLET5 cell line was grown in phenol red free DMEM supplemented with 10% DSS and 1% P/S/G. All cells were incubated at 37 °C in humidified 5% CO^2. FuGENE® HD transfection reagent was obtained from Roche (Burgess Hill, UK). Etoposide was purchased from Sigma Aldrich. The Dual-Glo™ Luciferase Assay System was purchased from Promega (Southampton, UK). The following antibodies have been used: KSR1 rabbit polyclonal (Santa Cruz and Cell Signaling), Anti-Flag mouse monoclonal (Sigma Aldrich), p53 mouse monoclonal DO-1 (Santa Cruz), Acetylated-p53 and phospho-p53 Ser15 rabbit polyclonal (Cell Signaling), BRCA1 rabbit polyclonal (Santa Cruz), BARD1 rabbit polyclonal (Cell Signaling), SIRT1 rabbit polyclonal (Santa Cruz), DBC1 and phospho-DBC1 Thr454 rabbit polyclonal (Cell Signaling), Ubiquitin mouse monoclonal (Cell Signaling) and β-actin mouse monoclonal (Abcam). The following p53-target gene promoter-reporter constructs previously described [53], were a kind gift from Prof. Kanaga Sabapathy: AIP-1-luciferase (luc), IGFBP3-luc, R2-luc and cyclinG1-luc. The renilla luciferase reporter vector (pRL-TK) was purchased from Promega (Southampton, UK).

Protein extraction and western blotting

NP40 lysis buffer (50 mM Tris-HCl, pH 8.0, 150 mM NaCl, 10%(v/v) glycerol, 1% NP40, 5 mM dithiothreitol (DTT), 1 mM EDTA, 1 mM EGTA, 50 μM leupeptin and 30 μg/ml aprotinin) was used to extract whole cell lysates. Cell pallets were mixed thoroughly with NP40 lysis buffer, and then incubated in ice for 15 min before centrifuging at 15000 rpm for 15 min at 4 °C. Nuclear and cytoplasmic extracts were prepared from whole-cell lysis using NE-PER Nuclear and Cytoplasmic Extraction Kit (Thermo Scientific). Protein concentration was measured by the bicinchoninic acid (BCA) protein assay (Pierce). Lysates were heated with 5x sodium dodecyl sulfates (SDS) sample buffer at 95 °C for 5 min before they were loaded to 10% SDS-PAGE. Samples were then transferred to Hybond ECL super nitrocellulose membranes (GE Healthcare). Subsequently the membranes were blocked in TBS containing 0.1% (v/v) Tween20 and 5% (w/v) non-fat milk for 1 h. The primary antibodies were probed with membranes overnight at 4 °C. The membranes were then washed three times in TBS/Tween for 15 min

following incubation with HRP-conjugated secondary antibodies (1:3000 dilution) for 60 min. The membranes were then washed three times again and were detected with Enhanced chemiluminescence (ECL). Films were developed using a Konica SRX-1001A X-ray developer. Alternatively, membranes were incubated with IRDye® Donkey anti-mouse or Donkey anti-rabbit secondary antibodies for 60 min and visualized by Odyssey® Fc Imaging System (LI-COR®).

RNA extraction and RT-qPCR

RNeasy kit (Qiagen) was used to isolate total RNA. Reverse transcription was performed using high capacity cDNA reverse transcription kit (Applied Biosystems). RT-qPCR analysis was performed on a 7900HT Thermocycler (Applied Biosystems) using TaqMan mastermix and primers for TP53, p21, KSR1, BRCA1 and GAPDH cDNAs, purchased from Applied Biosystems.

siRNA knock-down, constructs and generation of KSR1 stable cell lines

siKSR1 were purchased from Qiagen and verified. Plasmids containing human wild type KSR1 (pCMV6-KSR1) and empty vector (pCMV6-vector) were obtained from OriGene. MCF7-parental and MCF7-KSR1 stable cells were generated by transfection of either pCMV6-vector or pCMV6-KSR1 in MCF7 cells and selected in the presence of G418 (1 mg/ml). KSR1 overexpression was confirmed by RT-qPCR and western blotting.

Luciferase reporter assay

8×10^4/well MCF7 cells were seeded into 24-well plate and transfection was performed using FuGENE® HD transfection reagent according to manufacturer's instructions (Roche, UK). Cells were transfected with different p53 constructs, and pCMV6-KSR1 or pCMV6-vector and together with renilla luciferase reporter vector (pRL-TK). Cell lysates were collected after 24 hours transfection and firefly and renilla luciferase activities were measured by the Dual-Glo™ Luciferase Assay kit as manufacturer's protocols described. The transcriptional activity of various p53 constructs were determined by firefly luciferase activity and normalized against renilla luciferase activity which was served as control for transfection efficiency.

Three-dimensional overlay culture in Matrigel

Matrigel (BD Biosciences) was thawed on ice overnight at 4 ºC and 70 µl was added into each of the wells of the eight-well glass slide chambers (Thermo Scientific), and spread evenly in the

well to form a 1 mm thick bed. Matrigel was left to solidify at 37 ºC for 15 min. Next, cells (5 x 10^3/well) were plated in medium containing 2% Matrigel and allowed to grow in a 5% CO^2 humidified incubator at 37 $^{\circ}$C for 10 days. The assay medium containing 2% Matrigel was replaced every 4 days. Axiovert 100 MetaMorph microscope was used to image colonies in Matrigel.

Soft agar assay

Cells were plated in 0.3% agar on top of 0.6% agar in six-well plate in triplicates. Every 4 days, full DMEM medium with G418 (500 µg/ml) was replenished on the top layer. After incubation for 2 weeks, colonies were counted in 3 random fields per well and photographed.

Single nucleotide polymorphisms and genotyping

In those patients for whom adequate tissue was available, candidate KSR1 polymorphisms were chosen with the assistance of the Ensembl program using two main criteria: first, that the polymorphism has some degree of likelihood to alter the function of the gene in a biological relevant manner. Intronic or exonic polymorphisms can change gene transcription levels by alternative splicing or by affecting binding of a transcription factor. Second, that the frequency of the polymorphism is sufficient enough that its impact in clinical outcome would be meaningful on a population level (> 10% allele frequency). Genomic DNA was extracted from micro-dissected tissue specimens using the QIAamp kit (Qiagen). Two KSR1 polymorphisms (rs2241906 and rs1075952) were tested using polymerase chain reaction restriction fragment length polymorphism (PCR-RFLP) technique.

SILAC cell culture

SILAC dialysed calf serum and custom DMEM mediums containing either unlabelled [$^{12}C_6$,$^{14}N_4$]-arginine (Arg) and [$^{12}C_6$]-lysine (Lys) (R0K0 -'light') or labelled [$^{13}C_6$,$^{15}N_4$]-Arg and [$^{13}C_6$]-Lys (R10K8 -'heavy') were purchased from Dundee cell products (Dundee, UK) MCF7 cells were grown in these custom DMEM mediums along with 10% dialysed FCS and 1% of antibiotics (Penicillin and Streptomycin). The cells that were grown for at least seven passages were used for this experiment.

Neddylation assay

MCF7 cells plated on 15 cm dishes were transfected using FuGENE® HD with 8 µg pcDNA3-HA-NEDD8 (Addgene), 8 µg pCMV6-KSR1 or 8 µg pCMV6-Vector constructs as indicated.

After 24 hours, cells were lysed in Radio-Immunoprecipitation Assay (RIPA) buffer (Sigma Aldrich) supplemented with protease inhibitors. Total protein was quantified by the BCA assay (Pierce). 2 µg Mouse IgG or p53 (DO-1) was pre-incubated with protein agarose beads for 2 hours to form IP matrix complex (ImmunoCruz™ IP/WB Optima C System, Santa Cruz). 2 mg protein lysate was added into the beads and was incubated on a rotator overnight at 4 °C. Beads were washed with RIPA buffer for three times and were heated in SDS loading buffer. Neddylated p53 were detected by western blot using p53-specific DO-1 antibody or NEDD8 antibody (Cell Signalling) as described before[37,38].

Ubiquitination assay

MCF7 cells were transfected with pCMV6-KSR1 or pCMV6-Vector constructs using FuGENE® HD. After 24 hours, cells were lysed and total protein was quantified. Rabbit IgG or BRCA1 antibody was pre-incubated with protein agarose beads for 2 hours to form IP matrix complex (ImmunoCruz™ IP/WB Optima B System, Santa Cruz). 2 mg protein lysate was added into the beads and was incubated on a rotator overnight at 4 °C. Beads were then washed with RIPA buffer for three times and were heated in SDS loading buffer. Endogenous ubiquitinated BRCA1 was detected using anti-ubiquitin antibody by western blot.

Immunofluorescence staining

MCF7 cells seeded on glass coverslips in 6 cm dishes were transfected with pCMV6-KSR1 or pCMV6-Vector using FuGENE® HD. Cells were fixed in 4% w/v paraformaldehyde at 37 °C for 15 min, permeabilized with 0.1% Triton-X for 10 min and incubated in immune-fluorescent blocking buffer (10% AB-serum in PBS) for 1h, followed by incubation with p53 antibody (DO-1). After washing with PBS, coverslips were incubated for 45 min at 37 °C with anti-mouse-IgG Alexa Fluor® -555 antibody (Invitrogen). DNA was visualized by DAPI staining. Cells were examined on an Axiovert-200 laser scanning inverted microscope (Zeiss) as previously described [3].

References

1. Ali, S. & Coombes, R.C. Endocrine-responsive breast cancer and strategies for combating resistance. *Nature reviews. Cancer* 2, 101-112 (2002).
2. Stebbing, J. & Ngan, S. Breast cancer (metastatic). *Clinical evidence* 2010(2010).
3. Giamas, G.*, et al.* Kinome screening for regulators of the estrogen receptor identifies LMTK3 as a new therapeutic target in breast cancer. *Nat Med* 17, 715-719 (2011).
4. Therrien, M., Michaud, N.R., Rubin, G.M. & Morrison, D.K. KSR modulates signal propagation within the MAPK cascade. *Genes & development* 10, 2684-2695 (1996).
5. Xing, H., Kornfeld, K. & Muslin, A.J. The protein kinase KSR interacts with 14-3-3 protein and Raf. *Current biology : CB* 7, 294-300 (1997).
6. Michaud, N.R.*, et al.* KSR stimulates Raf-1 activity in a kinase-independent manner. *Proceedings of the National Academy of Sciences of the United States of America* 94, 12792-12796 (1997).
7. Zhang, Y.*, et al.* Kinase suppressor of Ras is ceramide-activated protein kinase. *Cell* 89, 63-72 (1997).
8. Kolesnick, R. & Xing, H.R. Inflammatory bowel disease reveals the kinase activity of KSR1. *The Journal of clinical investigation* 114, 1233-1237 (2004).
9. Zafrullah, M., Yin, X., Haimovitz-Friedman, A., Fuks, Z. & Kolesnick, R. Kinase suppressor of Ras transphosphorylates c-Raf-1. *Biochemical and biophysical research communications* 390, 434-440 (2009).
10. Goettel, J.A.*, et al.* KSR1 is a functional protein kinase capable of serine autophosphorylation and direct phosphorylation of MEK1. *Experimental cell research* 317, 452-463 (2011).
11. Hu, J.*, et al.* Mutation that blocks ATP binding creates a pseudokinase stabilizing the scaffolding function of kinase suppressor of Ras, CRAF and BRAF. *Proceedings of the National Academy of Sciences of the United States of America* 108, 6067-6072 (2011).
12. McKay, M.M., Ritt, D.A. & Morrison, D.K. Signaling dynamics of the KSR1 scaffold complex. *Proceedings of the National Academy of Sciences of the United States of America* 106, 11022-11027 (2009).
13. Yan, F.*, et al.* Kinase suppressor of Ras-1 protects intestinal epithelium from cytokine-mediated apoptosis during inflammation. *The Journal of clinical investigation* 114, 1272-1280 (2004).

14. Fusello, A.M.*, et al.* The MAPK scaffold kinase suppressor of Ras is involved in ERK activation by stress and proinflammatory cytokines and induction of arthritis. *J Immunol* 177, 6152-6158 (2006).
15. Zhang, Y.*, et al.* Kinase suppressor of Ras-1 protects against pulmonary Pseudomonas aeruginosa infections. *Nat Med* 17, 341-346 (2011).
16. Kortum, R.L. & Lewis, R.E. The molecular scaffold KSR1 regulates the proliferative and oncogenic potential of cells. *Molecular and cellular biology* 24, 4407-4416 (2004).
17. Xing, H.R.*, et al.* Pharmacologic inactivation of kinase suppressor of ras-1 abrogates Ras-mediated pancreatic cancer. *Nat Med* 9, 1266-1268 (2003).
18. Adjei, A.A. Blocking oncogenic Ras signaling for cancer therapy. *Journal of the National Cancer Institute* 93, 1062-1074 (2001).
19. Levine, A.J. p53, the cellular gatekeeper for growth and division. *Cell* 88, 323-331 (1997).
20. Vogelstein, B., Lane, D. & Levine, A.J. Surfing the p53 network. *Nature* 408, 307-310 (2000).
21. Brooks, C.L. & Gu, W. Ubiquitination, phosphorylation and acetylation: the molecular basis for p53 regulation. *Current opinion in cell biology* 15, 164-171 (2003).
22. Tang, Y., Zhao, W., Chen, Y., Zhao, Y. & Gu, W. Acetylation is indispensable for p53 activation. *Cell* 133, 612-626 (2008).
23. Kim, J.E., Chen, J. & Lou, Z. DBC1 is a negative regulator of SIRT1. *Nature* 451, 583-586 (2008).
24. Zhao, W.*, et al.* Negative regulation of the deacetylase SIRT1 by DBC1. *Nature* 451, 587-590 (2008).
25. Yuan, J., Luo, K., Liu, T. & Lou, Z. Regulation of SIRT1 activity by genotoxic stress. *Genes & development* 26, 791-796 (2012).
26. Zannini, L., Buscemi, G., Kim, J.E., Fontanella, E. & Delia, D. DBC1 phosphorylation by ATM/ATR inhibits SIRT1 deacetylase in response to DNA damage. *Journal of molecular cell biology* 4, 294-303 (2012).
27. Miki, Y.*, et al.* A strong candidate for the breast and ovarian cancer susceptibility gene BRCA1. *Science* 266, 66-71 (1994).
28. Wu, L.C.*, et al.* Identification of a RING protein that can interact in vivo with the BRCA1 gene product. *Nature genetics* 14, 430-440 (1996).

29. Choudhury, A.D., Xu, H. & Baer, R. Ubiquitination and proteasomal degradation of the BRCA1 tumor suppressor is regulated during cell cycle progression. *J Biol Chem* 279, 33909-33918 (2004).
30. Xia, Y., Pao, G.M., Chen, H.W., Verma, I.M. & Hunter, T. Enhancement of BRCA1 E3 ubiquitin ligase activity through direct interaction with the BARD1 protein. *J Biol Chem* 278, 5255-5263 (2003).
31. Rhodes, D.R.*, et al.* ONCOMINE: a cancer microarray database and integrated data-mining platform. *Neoplasia* 6, 1-6 (2004).
32. Finak, G.*, et al.* Stromal gene expression predicts clinical outcome in breast cancer. *Nat Med* 14, 518-527 (2008).
33. Karnoub, A.E.*, et al.* Mesenchymal stem cells within tumour stroma promote breast cancer metastasis. *Nature* 449, 557-563 (2007).
34. Ma, X.J., Dahiya, S., Richardson, E., Erlander, M. & Sgroi, D.C. Gene expression profiling of the tumor microenvironment during breast cancer progression. *Breast cancer research : BCR* 11, R7 (2009).
35. Richardson, A.L.*, et al.* X chromosomal abnormalities in basal-like human breast cancer. *Cancer cell* 9, 121-132 (2006).
36. Cox, J. & Mann, M. MaxQuant enables high peptide identification rates, individualized p.p.b.-range mass accuracies and proteome-wide protein quantification. *Nature biotechnology* 26, 1367-1372 (2008).
37. Xirodimas, D.P., Saville, M.K., Bourdon, J.C., Hay, R.T. & Lane, D.P. Mdm2-mediated NEDD8 conjugation of p53 inhibits its transcriptional activity. *Cell* 118, 83-97 (2004).
38. Abida, W.M., Nikolaev, A., Zhao, W., Zhang, W. & Gu, W. FBXO11 promotes the Neddylation of p53 and inhibits its transcriptional activity. *J Biol Chem* 282, 1797-1804 (2007).
39. Kornfeld, K., Hom, D.B. & Horvitz, H.R. The ksr-1 gene encodes a novel protein kinase involved in Ras-mediated signaling in C. elegans. *Cell* 83, 903-913 (1995).
40. Therrien, M.*, et al.* KSR, a novel protein kinase required for RAS signal transduction. *Cell* 83, 879-888 (1995).
41. Rajakulendran, T., Sahmi, M., Lefrancois, M., Sicheri, F. & Therrien, M. A dimerization-dependent mechanism drives RAF catalytic activation. *Nature* 461, 542-545 (2009).
42. McKay, M.M., Ritt, D.A. & Morrison, D.K. RAF inhibitor-induced KSR1/B-RAF binding and its effects on ERK cascade signaling. *Current biology : CB* 21, 563-568 (2011).

43. Lozano, J.*, et al.* Deficiency of kinase suppressor of Ras1 prevents oncogenic ras signaling in mice. *Cancer research* 63, 4232-4238 (2003).
44. Zhang, J.*, et al.* Downregulation of KSR1 in pancreatic cancer xenografts by antisense oligonucleotide correlates with tumor drug uptake. *Cancer biology & therapy* 7, 1490-1495 (2008).
45. Vaziri, H.*, et al.* hSIR2(SIRT1) functions as an NAD-dependent p53 deacetylase. *Cell* 107, 149-159 (2001).
46. Elston, C.W. & Ellis, I.O. Pathological prognostic factors in breast cancer. I. The value of histological grade in breast cancer: experience from a large study with long-term follow-up. *Histopathology* 19, 403-410 (1991).
47. Dalton, L.W.*, et al.* Histologic grading of breast cancer: linkage of patient outcome with level of pathologist agreement. *Modern pathology : an official journal of the United States and Canadian Academy of Pathology, Inc* 13, 730-735 (2000).
48. Stebbing, J.*, et al.* LMTK3 expression in breast cancer: association with tumor phenotype and clinical outcome. *Breast Cancer Res Treat* 132, 537-544 (2012).
49. Zhang, H.*, et al.* The proteins FABP7 and OATP2 are associated with the basal phenotype and patient outcome in human breast cancer. *Breast Cancer Res Treat* 121, 41-51 (2010).
50. Wisniewski, J.R., Zougman, A., Nagaraj, N. & Mann, M. Universal sample preparation method for proteome analysis. *Nature methods* 6, 359-362 (2009).
51. Thingholm, T.E., Jorgensen, T.J., Jensen, O.N. & Larsen, M.R. Highly selective enrichment of phosphorylated peptides using titanium dioxide. *Nature protocols* 1, 1929-1935 (2006).
52. Cox, J.*, et al.* Andromeda: a peptide search engine integrated into the MaxQuant environment. *Journal of proteome research* 10, 1794-1805 (2011).
53. Vikhanskaya, F., Lee, M.K., Mazzoletti, M., Broggini, M. & Sabapathy, K. Cancer-derived p53 mutants suppress p53-target gene expression--potential mechanism for gain of function of mutant p53. *Nucleic Acids Res* 35, 2093-2104 (2007).

Figure 1

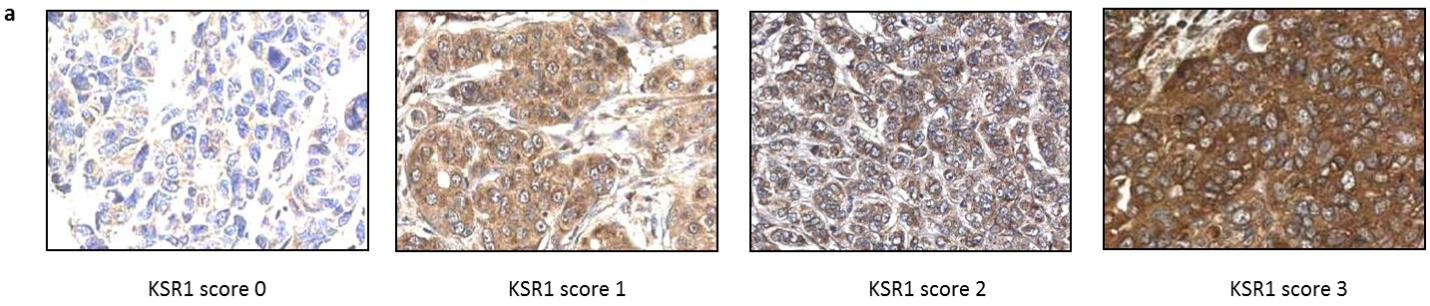
a
KSR1 score 0
KSR1 score 1
KSR1 score 2
KSR1 score 3

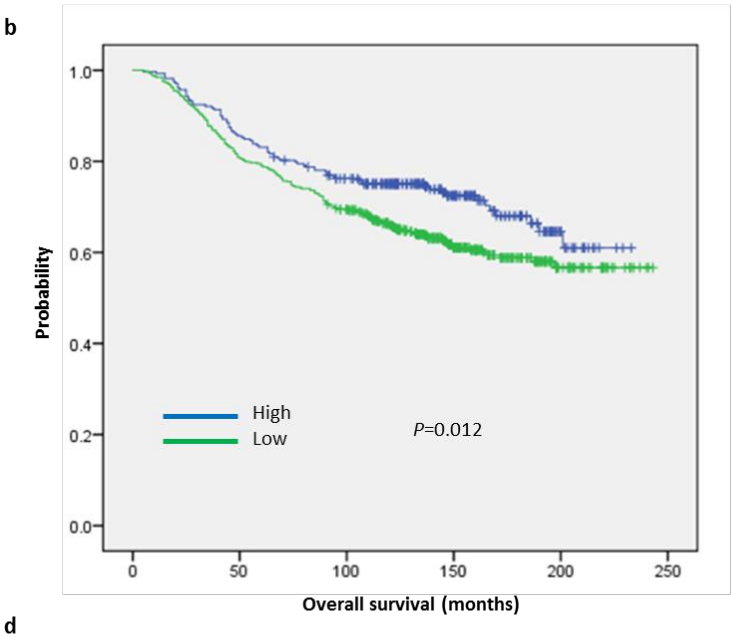
b
Probability
1.0
0.8
0.6
0.4
0.2
0.0
0
50
100
150
200
250
Overall survival (months)
High
Low
P=0.012

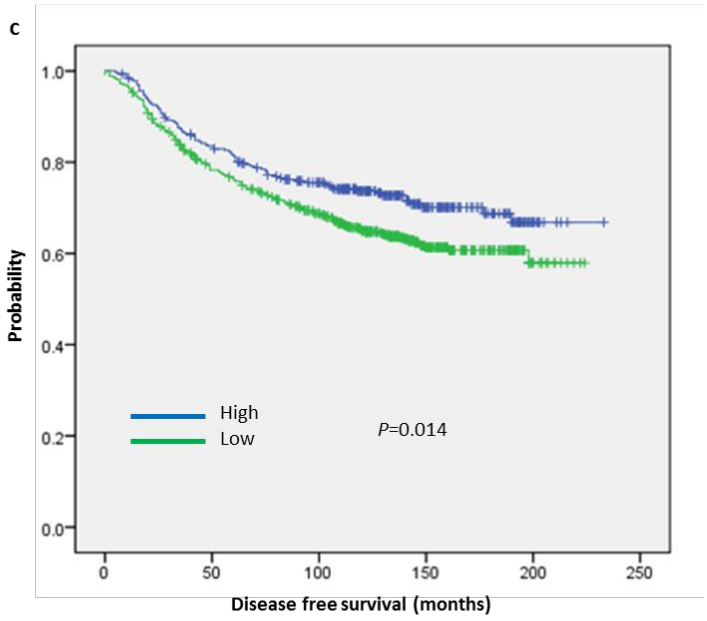
c
Probability
1.0
0.8
0.6
0.4
0.2
0.0
0
50
100
150
200
250
Disease free survival (months)
High
Low
P=0.014

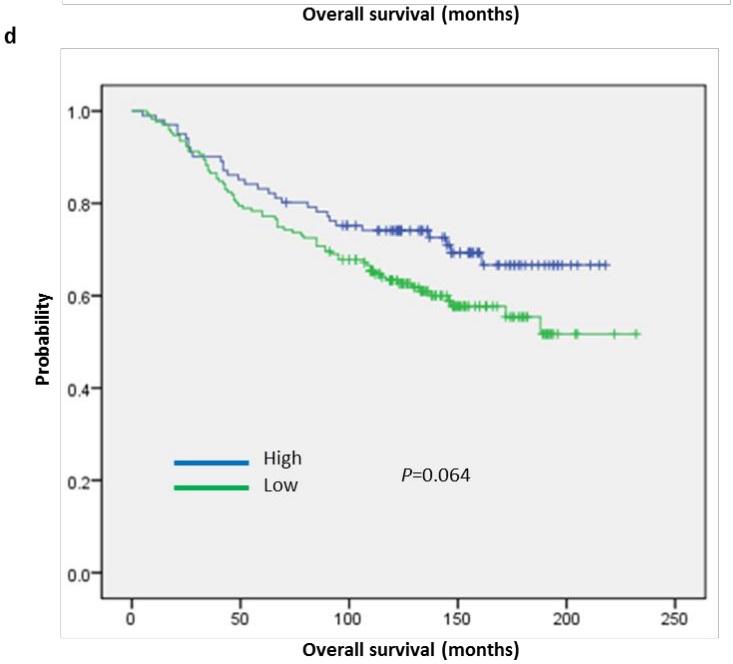
d
Probability
1.0
0.8
0.6
0.4
0.2
0.0
0
50
100
150
200
250
Overall survival (months)
High
Low
P=0.064

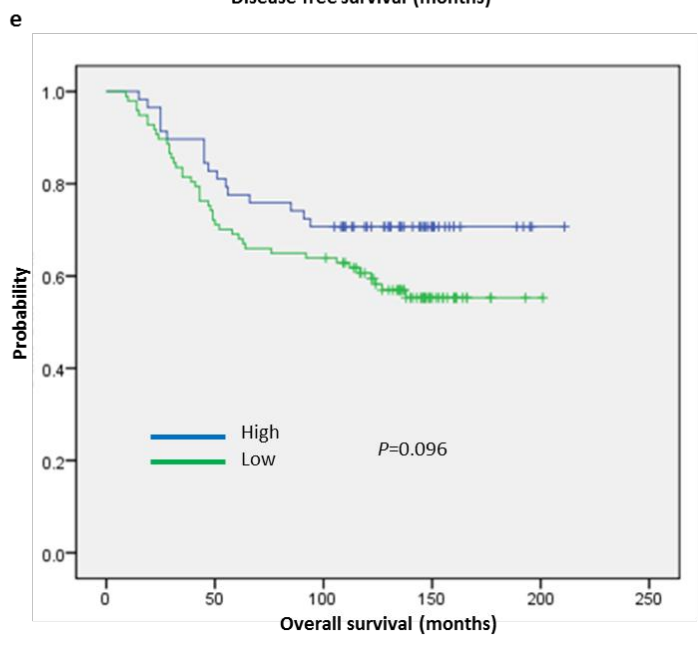
e
Probability
1.0
0.8
0.6
0.4
0.2
0.0
0
50
100
150
200
250
Overall survival (months)
High
Low
P=0.096

Figure 2

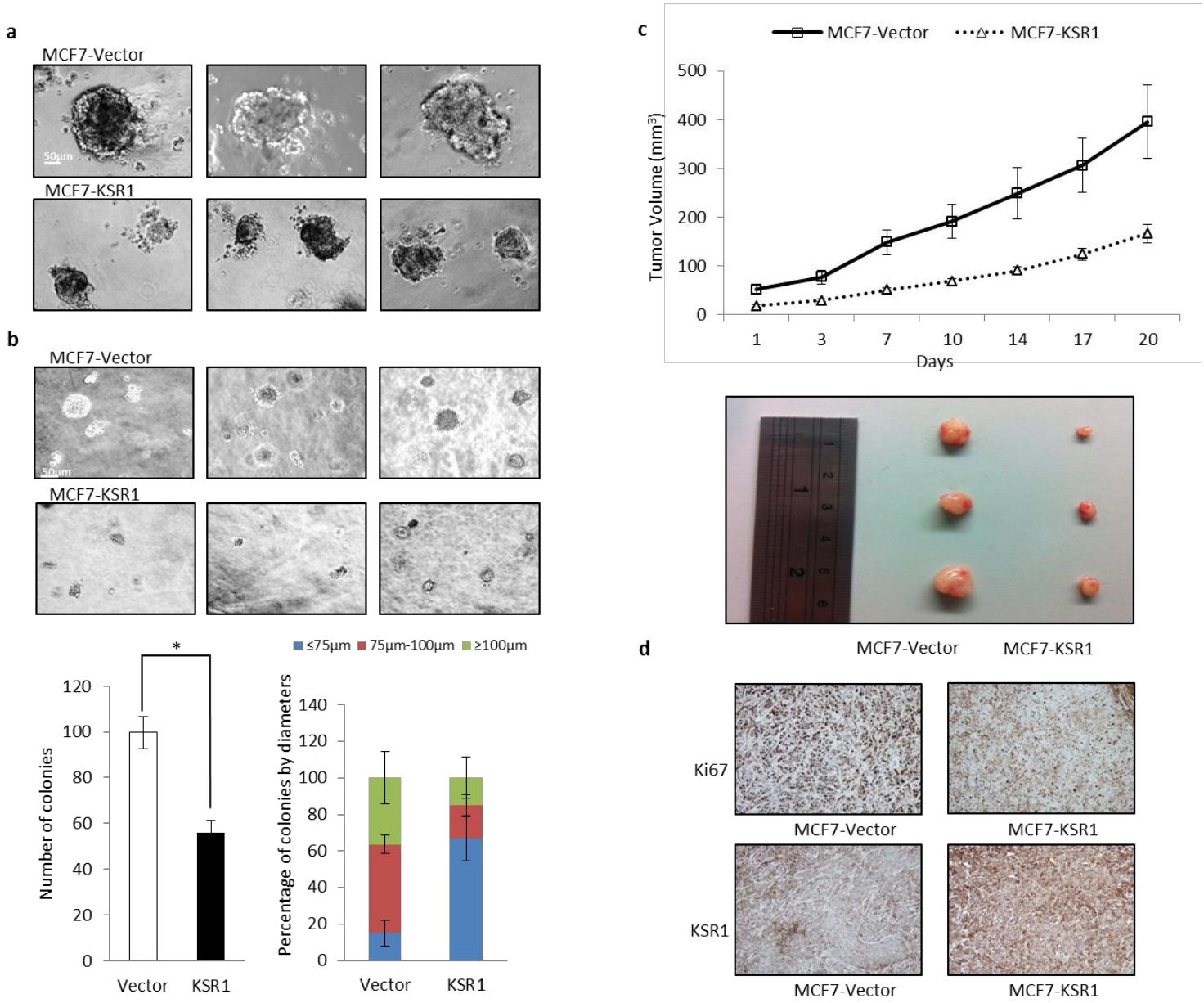
a
MCF7-Vector
50μm
MCF7-KSR1
b
MCF7-Vector
50μm
MCF7-KSR1
*
Number of colonies
120
100
80
60
40
20
0
Vector
KSR1
≤75μm
75μm-100μm
≥100μm
Percentage of colonies by diameters
140
120
100
80
60
40
20
0
Vector
KSR1
c
MCF7-Vector
MCF7-KSR1
Tumor Volume (mm³)
500
400
300
200
100
0
1
3
7
10
14
17
20
Days
MCF7-Vector
MCF7-KSR1
d
Ki67
MCF7-Vector
MCF7-KSR1
KSR1
MCF7-Vector
MCF7-KSR1

Figure 3

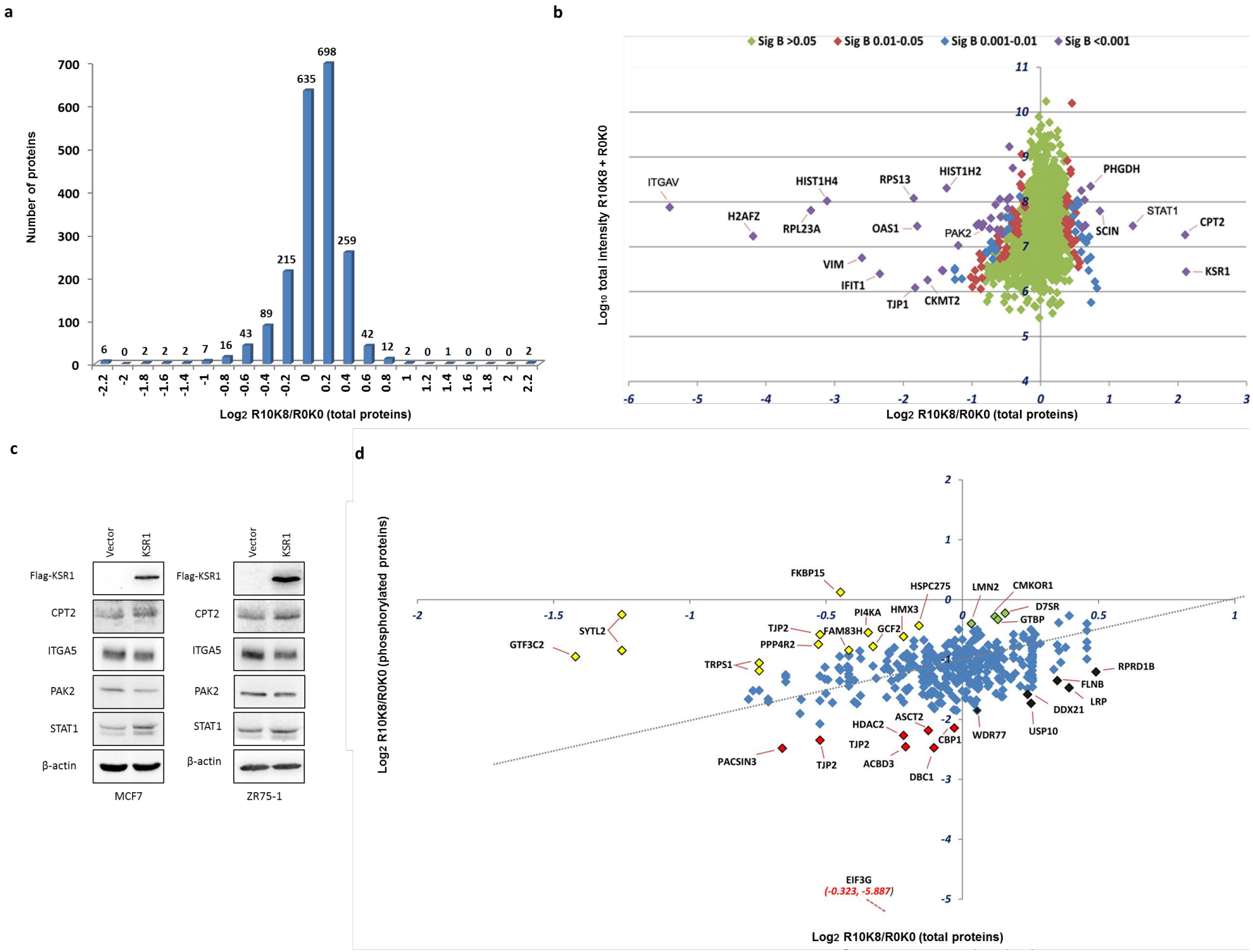
a
Number of proteins
Log2 R10K8/R0K0 (total proteins)
b
Sig B >0.05
Sig B 0.01-0.05
Sig B 0.001-0.01
Sig B <0.001
Log10 total intensity R10K8 + R0K0
Log2 R10K8/R0K0 (total proteins)
ITGAV
HIST1H4
RPS13
HIST1H2
PHGDH
H2AFZ
RPL23A
OAS1
PAK2
SCIN
STAT1
CPT2
VIM
IFIT1
TJP1
CKMT2
KSR1
c
Vector
KSR1
Flag-KSR1
CPT2
ITGA5
PAK2
STAT1
β-actin
MCF7
ZR75-1
d
Log2 R10K8/R0K0 (phosphorylated proteins)
Log2 R10K8/R0K0 (total proteins)
FKBP15
HSPC275
LMN2
CMKOR1
D7SR
GTBP
SYTL2
GTF3C2
TJP2
FAM83H
PI4KA
HMX3
GCF2
PPP4R2
TRPS1
RPRD1B
FLNB
LRP
DDX21
USP10
WDR77
ASCT2
HDAC2
CBP1
TJP2
ACBD3
PACSIN3
TJP2
DBC1
EIF3G
(-0.323, -5.887)

Figure 4

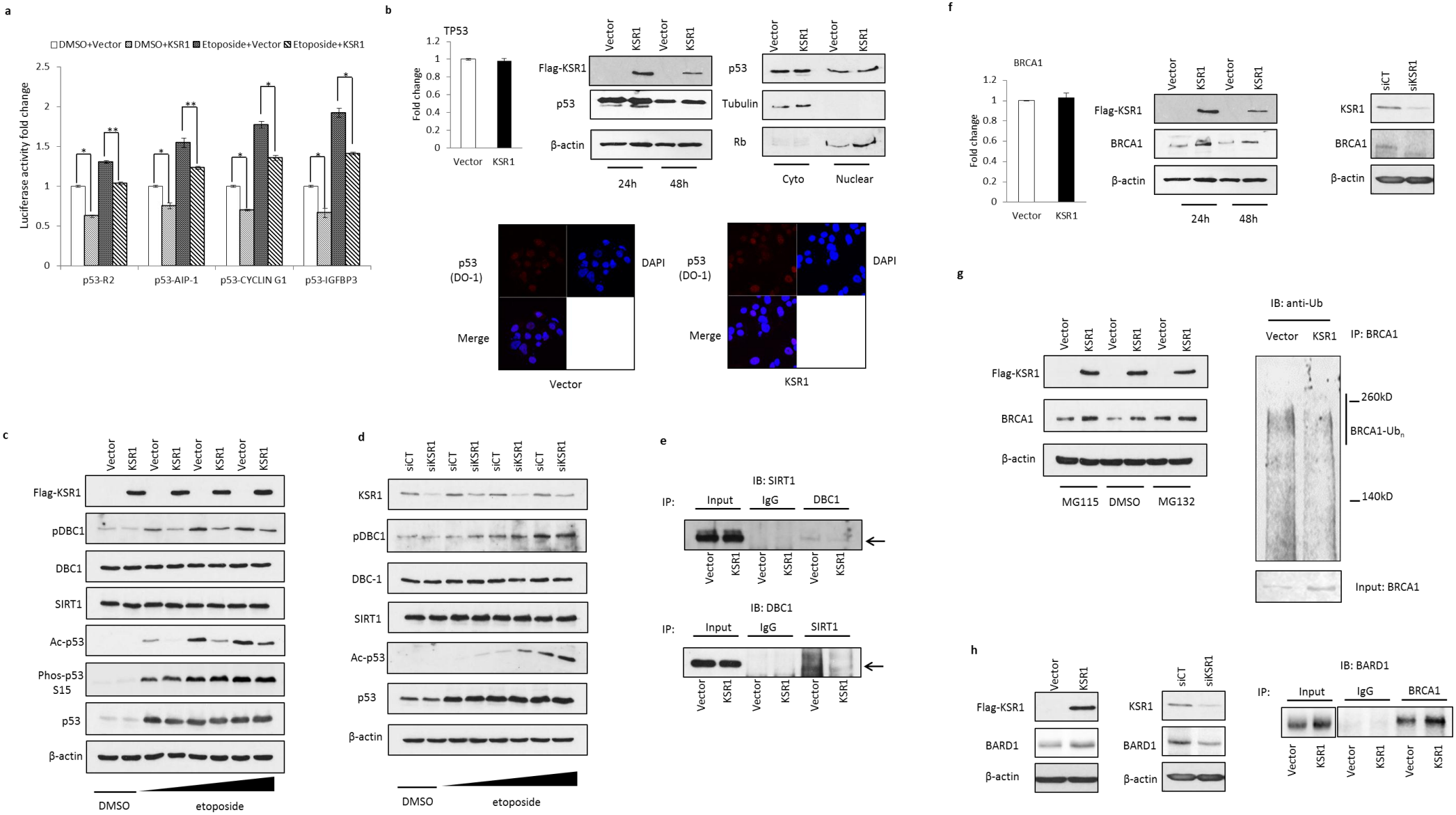
a
DMSO+Vector
DMSO+KSR1
Etoposide+Vector
Etoposide+KSR1
Luciferase activity fold change
p53-R2
p53-AIP-1
p53-CYCLIN G1
p53-IGFBP3
b
TP53
Fold change
Vector
KSR1
Flag-KSR1
p53
β-actin
24h
48h
Tubulin
Rb
Cyto
Nuclear
p53 (DO-1)
DAPI
Merge
c
Flag-KSR1
pDBC1
DBC1
SIRT1
Ac-p53
Phos-p53 S15
DMSO
etoposide
d
siCT
siKSR1
KSR1
pDBC1
DBC-1
SIRT1
Ac-p53
p53
β-actin
e
IB: SIRT1
IP:
Input
IgG
DBC1
IB: DBC1
SIRT1
f
BRCA1
Flag-KSR1
BRCA1
β-actin
siKSR1
g
IB: anti-Ub
IP: BRCA1
260kD
BRCA1-Ub$_n$
140kD
Input: BRCA1
MG115
DMSO
MG132
h
BARD1
IB: BARD1

Figure 5

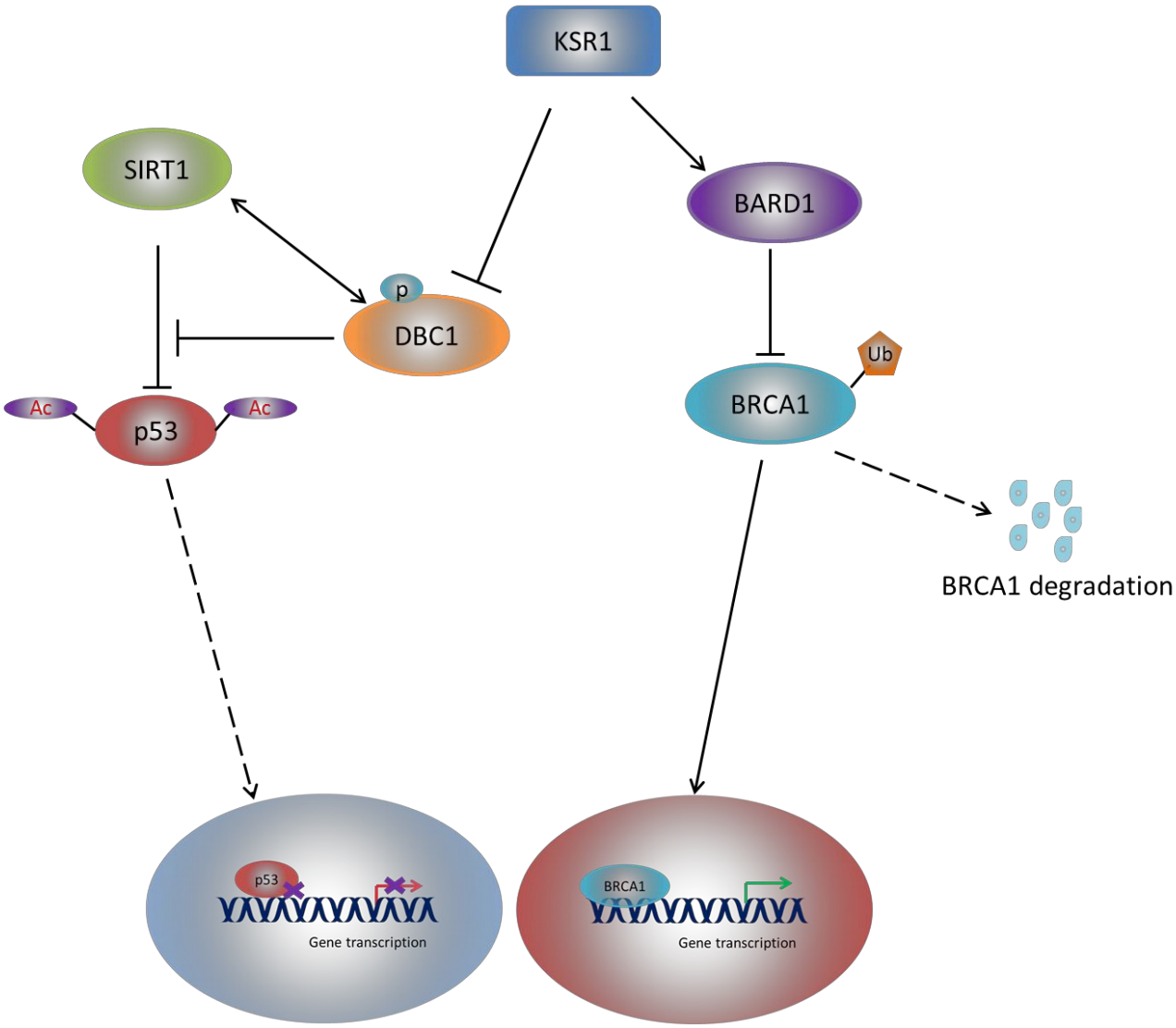
KSR1
SIRT1
BARD1
p
DBC1
Ac
p53
Ac
Ub
BRCA1
BRCA1 degradation
p53
Gene transcription
BRCA1
Gene transcription

Supplementary Figure 1

a

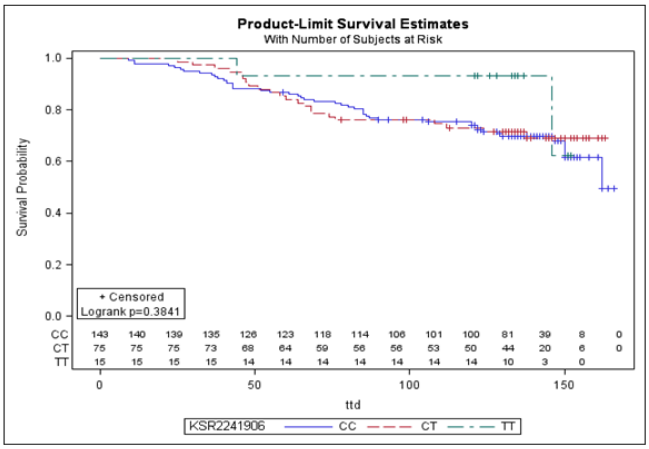

Overall survival

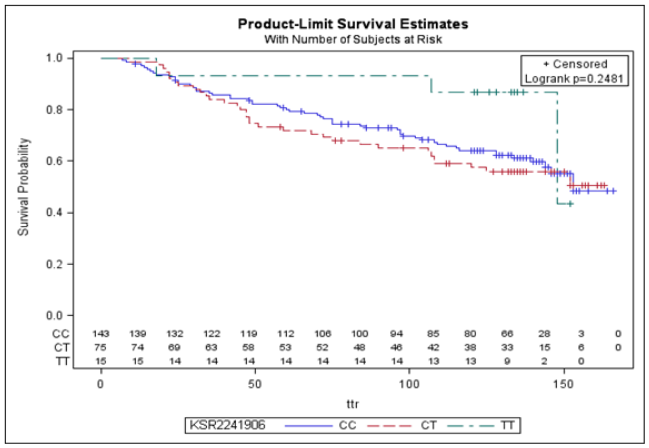

Disease free survival

b

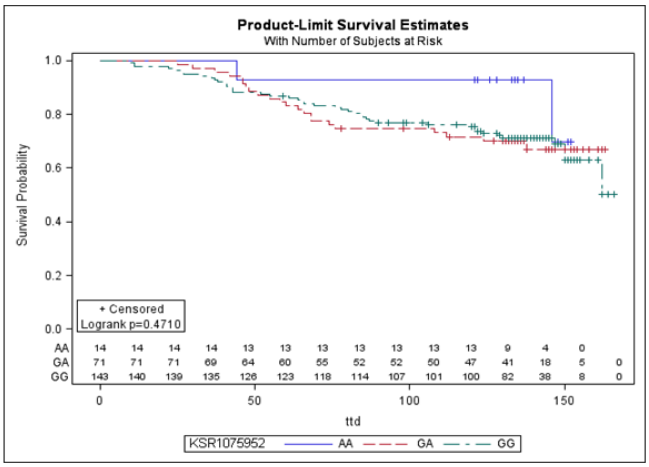

Overall survival

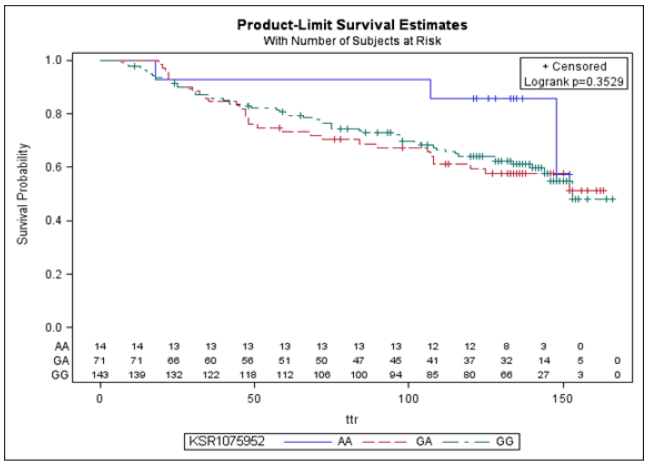

Disease free survival

Supplementary Figure 2

Finak dataset

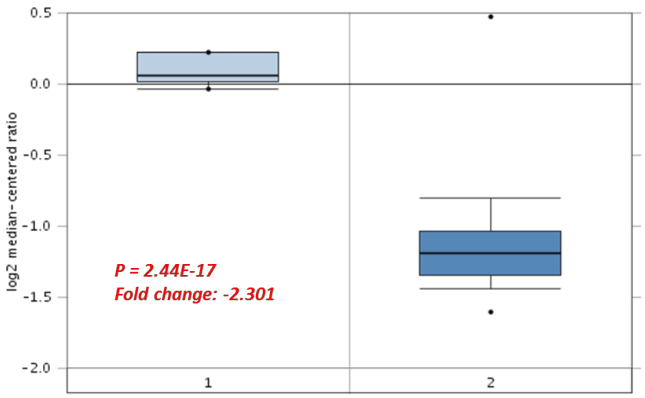

1. Breast
2. Invasive breast carcinoma

Karnoub dataset

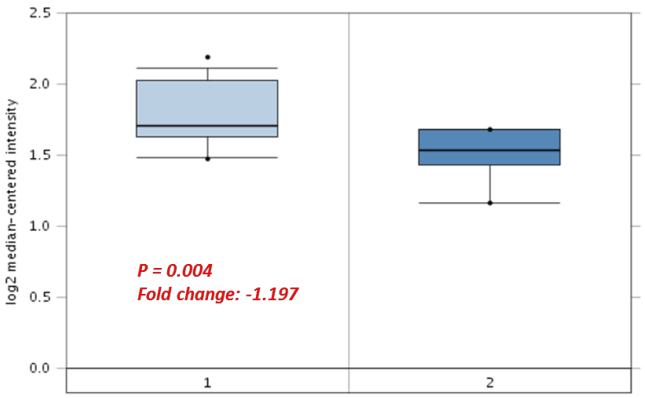

1. Breast (
2. Invasive ductal breast carcinoma

Ma dataset

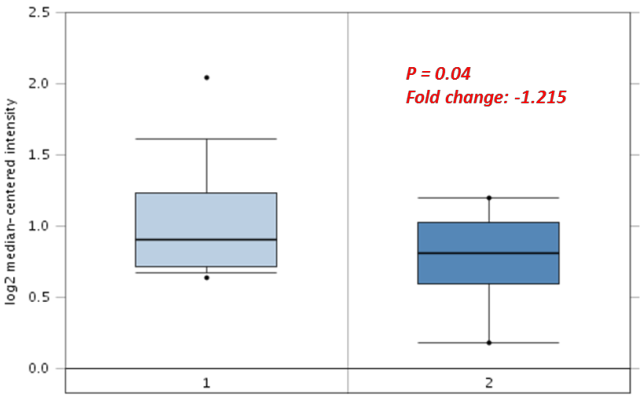

1. Breast
2. Invasive ductal breast carcinoma

Richardson dataset

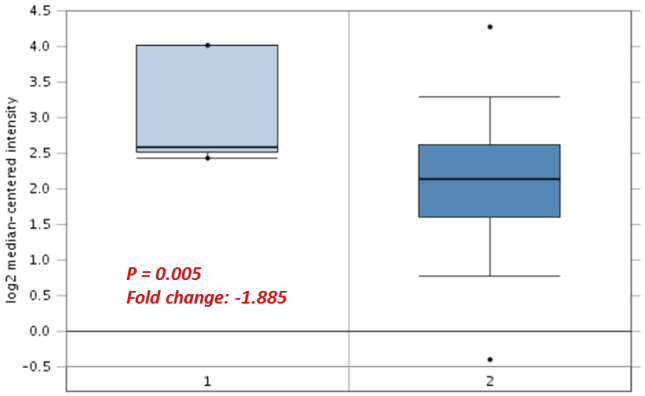

1. Breast
2. Ductal breast carcinoma

Supplementary Figure 3

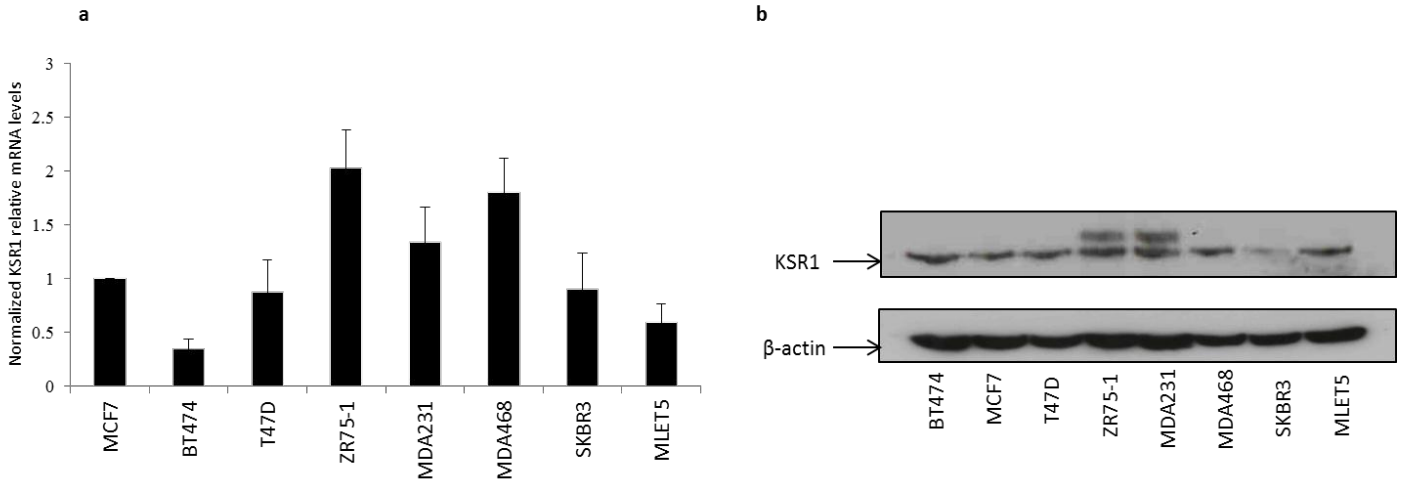

Supplementary Figure 4

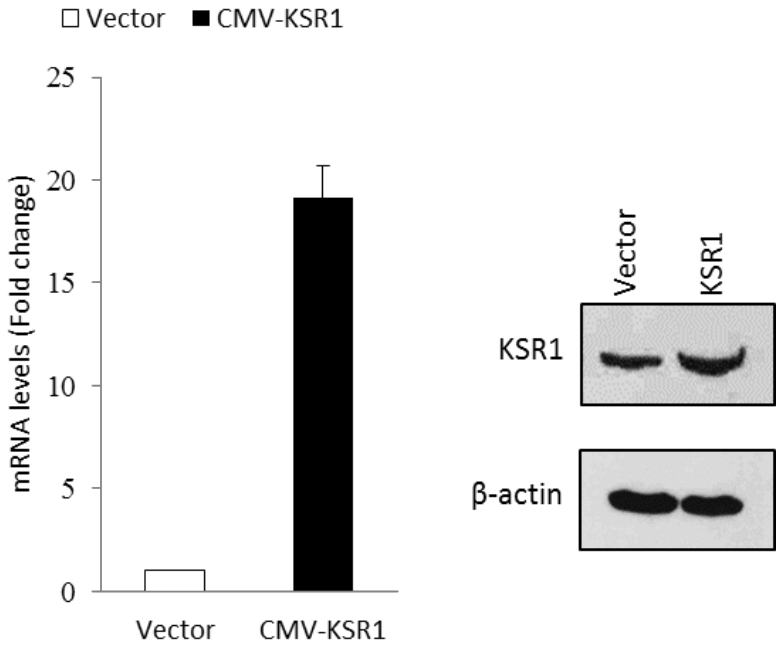

Supplementary Figure 5

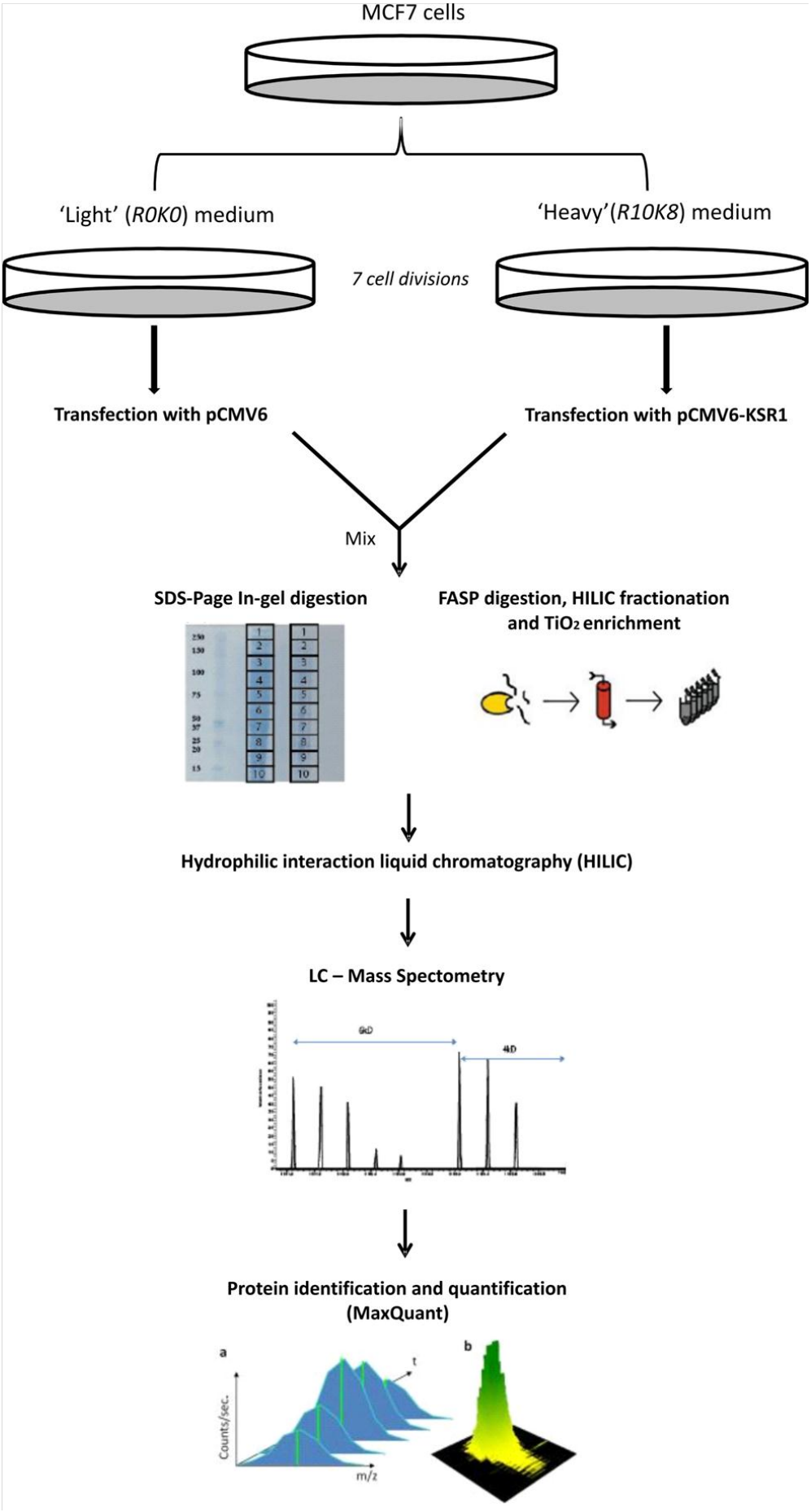

Supplementary Figure 6

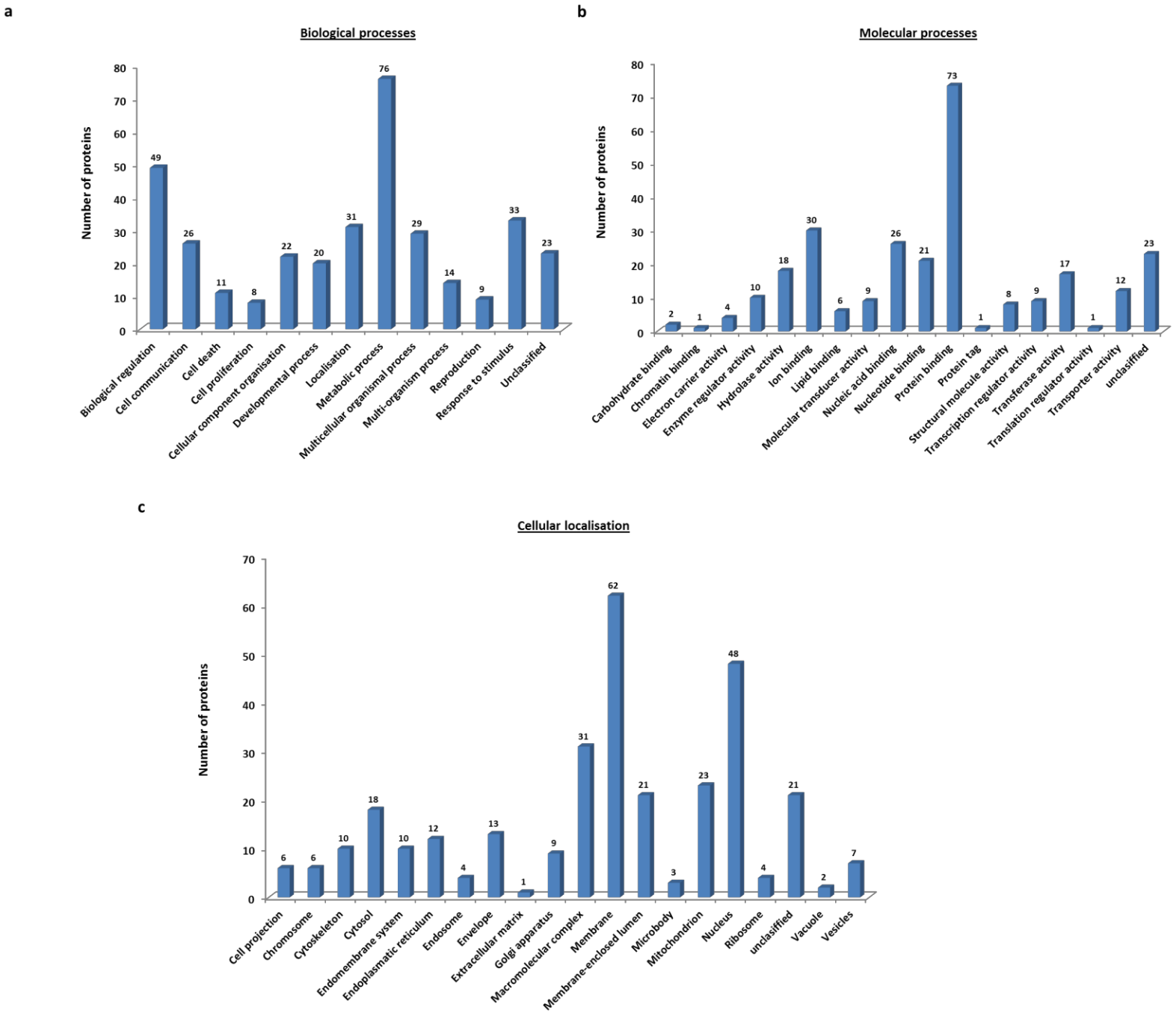

Supplementary Figure 7

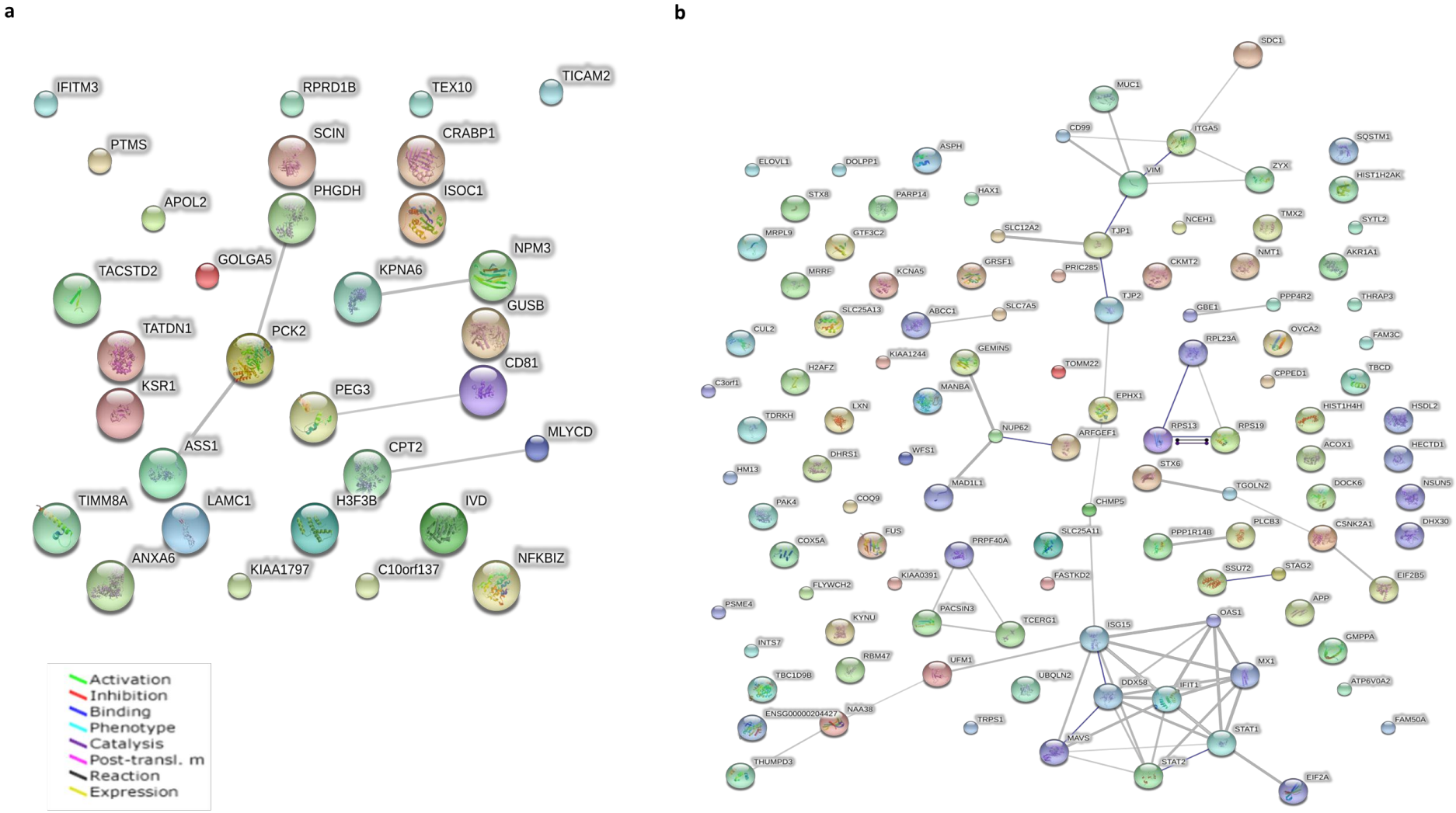

Supplementary Figure 8

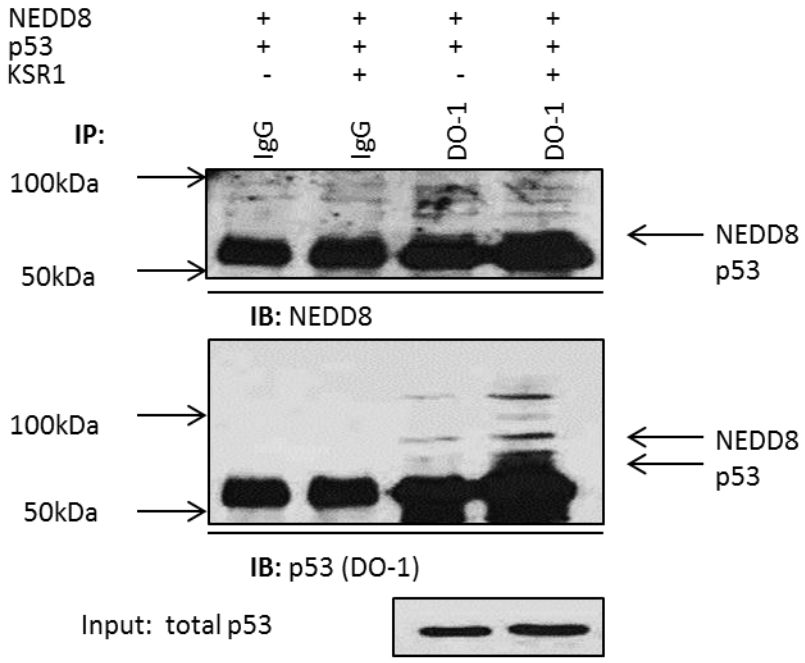

Supplementary Figure 9

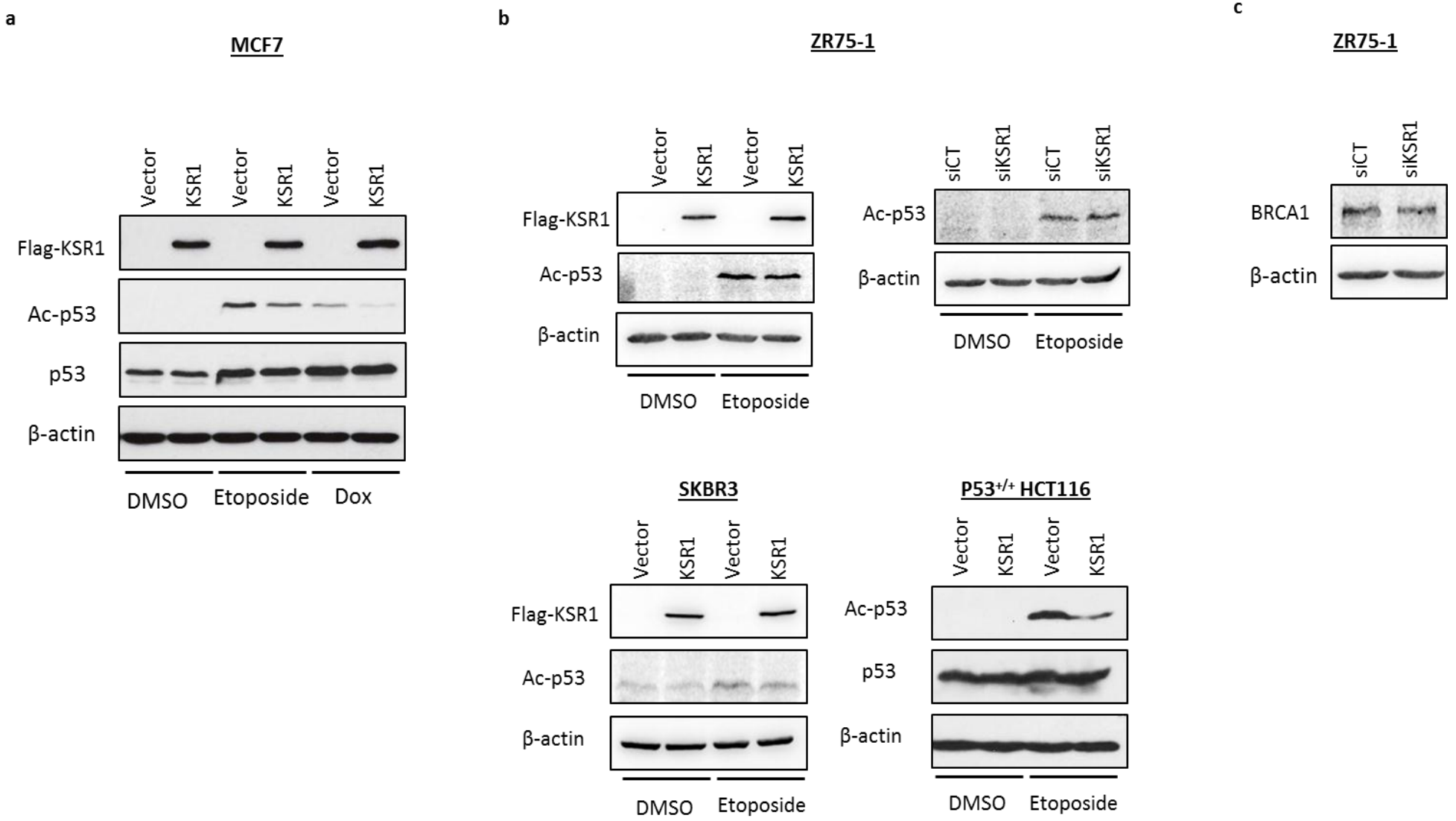

Table 1. Patients' characteristics and tumor biomarkers and correlations with KSR1 expression in European breast cancer patients.

	KSR1 expression		*P* value
Variable/biomarker	Weak (%)	Strong (%)	
Tumor Stage			
1	370(59.7)	191(58.2)	0.787
2	194(31.3)	103(31.4)	
3	56(9.0)	34(10.4)	
Grade			
1	95(15.3)	42(12.8)	0.544
2	199(32.0)	104(31.7)	
3	328(52.7)	182(55.5)	
Tumor Size			
<1.5cm	141(22.7)	71(21.6)	0.719
=>1.5cm	481(77.3)	257(78.4)	
Age			
<50	197(31.6)	120(36.6)	0.119
=>50	427(68.4)	208(63.4)	
Vascular Invasion			
Definitive	217(34.9)	115(35.6)	0.973
Negative	326(52.4)	168(52.0)	
Probable	79(12.7)	40(12.4)	
Tumor type			
Invasive Ductal	376(61.3)	215(67.0)	0.180
Other	237(38.7)	106(33.1)	
***ER* Status**			
Negative	167(27.5)	103(32.2)	0.149
Positive	440(72.5)	217(67.7)	
***PgR* Status**			
Negative	258(43.1)	144(45.9)	0.420
Positive	341(56.9)	170(54.1)	
***HER2* Status**			
Negative	521(85.4)	273(84.3)	0.639
Positive	89(14.6)	51(15.7)	
Triple Negative Status			
Non-Triple	493(81.9)	249(77.8)	0.137
Triple Negative	109(18.1)	71(22.2)	
Cytokeratin 5/6			
Negative	504(83.3)	260(81.8)	0.555
Positive	101(16.7)	58(18.2)	
Cytokeratin 14			
Negative	522(86.4)	273(86.7)	0.919
Positive	82(13.6)	42(13.3)	
BRCA1			
0	100(20.0)	40(15.2)	0.002
1	222(44.4)	96(36.4)	
2	178(35.6)	128(48.5)	
P53			
0	332(69.7)	200(76.9)	0.038
1	144(30.3)	60(23.1)	
Ki67			
0	175(42.0)	79(36.1)	0.149
1	242(58.0)	140(63.9)	

Table 2. Cox-proportional hazards analysis for predictors (model including KSR1 expression) of overall survival (OS) and disease-free survival (DFS)

Variable	OS			DFS		
	Hazard ratio	95% CI	*P* value	Hazard ratio	95% CI	*P* value
Stage[a]	1.846	1.562-2.180	<0.001	1.893	1.585-2.260	<0.001
Grade[b]	1.755	1.435-2.146	<0.001	2.222	1.747-2.825	<0.001
Size>1.5 cm[c]	1.825	1.246-2.674	0.002	2.026	1.310-3.134	0.002
KSR1 status	1.543	1.189-2.001	0.001	1.541	1.166-2.037	0.002

a Fitted as linear term, i.e., Increase in risk for change in lymph node stage of one unit
b Fitted as linear term, i.e., Increase in risk for change in grade of one unit
c Compared with tumour size ≤1.5cm

Supplementary Table 1. SILAC KSR1-upregulated proteins (- log_2 >0.5 fold).

Protein IDs	Protein Descriptions	Normalised R10K8/R0K0	Log_2 R10K8/R0K0
IPI00651657	Isoform 1 of Kinase suppressor of Ras 1	***4.3486***	***2.1205***
IPI00012912	Carnitine O-palmitoyltransferase 2, mitochondrial	***4.3074***	***2.1068***
IPI00030781	Isoform Alpha of Signal transducer and activator of transcription 1-alpha/beta	***2.5401***	***1.3450***
IPI00002606	Isoform 1 of Adseverin	***1.8201***	***0.8640***
IPI00296922	Laminin subunit beta-2	***1.7680***	***0.8221***
IPI00748360	Uncharacterized protein KIAA1797	***1.7324***	***0.7928***
IPI00220007	cDNA FLJ55764, highly similar to Apolipoprotein-L2	***1.6657***	***0.7361***
IPI00028376	Mitochondrial import inner membrane translocase subunit Tim8 A	***1.6590***	***0.7304***
IPI00011200	D-3-phosphoglycerate dehydrogenase	***1.6582***	***0.7297***
IPI00027745	Isoform Long of Beta-glucuronidase	***1.6364***	***0.7105***
IPI00000663	Isoform Mitochondrial of Malonyl-CoA decarboxylase, mitochondrial	***1.6268***	***0.7021***
IPI00549664	Testis-expressed sequence 10 protein	***1.6001***	***0.6782***
IPI00027741	Isoform 1 of NF-kappa-B inhibitor zeta	***1.5888***	***0.6680***
IPI00304082	Isochorismatase domain-containing protein 1	***1.5729***	***0.6534***
IPI00183110	Isoform 1 of Paternally-expressed gene 3 protein	***1.5601***	***0.6416***
IPI00428967	TRAM adaptor with GOLD domain isoform 1	***1.5321***	***0.6155***
IPI00297910	Tumor-associated calcium signal transducer 2	***1.5232***	***0.6071***
IPI00789848	isovaleryl Coenzyme A dehydrogenase isoform 1	***1.5144***	***0.5988***
IPI00797038	mitochondrial phosphoenolpyruvate carboxykinase 2 isoform 1 precursor	***1.5086***	***0.5932***
IPI00303726	Interferon-induced transmembrane protein 3	***1.5076***	***0.5923***
IPI00550020	Parathymosin	***1.4883***	***0.5737***
IPI00386227	cDNA: FLJ21617 fis, clone COL07481	***1.4746***	***0.5603***
IPI00020632	Argininosuccinate synthase	***1.4657***	***0.5516***
IPI00219930	Cellular retinoic acid-binding protein 1	***1.4642***	***0.5501***
IPI00219038	Histone H3.3	***1.4490***	***0.5351***
IPI00002459	annexin VI isoform 2	***1.4483***	***0.5344***
IPI00657752	Putative uncharacterized protein CD81	***1.4418***	***0.5279***
IPI00795107	Similar to Deoxyribonuclease	***1.4324***	***0.5185***
IPI00294065	Isoform 1 of Golgin subfamily A member 5	***1.4277***	***0.5137***
IPI00026496	Nucleoplasmin-3	***1.4238***	***0.5098***
IPI00009659	Regulation of nuclear pre-mRNA domain-containing protein 1B	***1.4051***	***0.4907***

Supplementary Table 2. SILAC_KSR1-downregulated proteins (- log_2 <0.5 fold).

Protein IDs	Protein Descriptions	Normalised R10K8/R0K0	Log_2 R10K8/R0K0
IPI00027505	Isoform 1 of Integrin alpha-V	*0.0237*	*-5.4019*
IPI00913961	18 kDa protein	*0.0550*	*-4.1856*
IPI00789159	Ribosomal protein L23a, isoform CRA_a	*0.0984*	*-3.3446*
IPI00453473	Histone H4	*0.1158*	*-3.1097*
IPI00418471	Vimentin	*0.1647*	*-2.6024*
IPI00018300	Interferon-induced protein with tetratricopeptide repeats 1	*0.1973*	*-2.3413*
IPI00221089	40S ribosomal protein S13	*0.2779*	*-1.8471*
IPI00216219	Isoform Long of Tight junction protein ZO-1	*0.2821*	*-1.8256*
IPI00651622	2-5 oligoadenylate synthetase 1 p52 isoform	*0.2880*	*-1.7956*
IPI00015141	Creatine kinase S-type, mitochondrial	*0.3200*	*-1.6441*
IPI00657888	Isoform 2 of Mannose-1-phosphate guanyltransferase alpha	*0.3699*	*-1.4349*
IPI00878252	Isoform 1 of General transcription factor 3C polypeptide 2	*0.3738*	*-1.4197*
IPI00291764	Histone H2A type 1	*0.3873*	*-1.3684*
IPI00935700	Isoform 13 of Synaptotagmin-like protein 2	*0.4207*	*-1.2493*
IPI00743871	Isoform 1 of Integrator complex subunit 7	*0.4213*	*-1.2471*
IPI00000425	V-type proton ATPase 116 kDa subunit a isoform 2	*0.4215*	*-1.2464*
IPI00002441	Syndecan-1	*0.4355*	*-1.1992*
IPI00299387	Transmembrane protein C3orf1	*0.4518*	*-1.1462*
IPI00060521	FLYWCH family member 2	*0.4950*	*-1.0145*
IPI00719178	Isoform 9 of Multidrug resistance-associated protein 1	*0.5023*	*-0.9934*
IPI00306127	THUMP domain-containing protein 3	*0.5163*	*-0.9539*
IPI00470883	stromal antigen 2 isoform a	*0.5190*	*-0.9461*
IPI00006608	Isoform APP770 of Amyloid beta A4 protein (Fragment)	*0.5199*	*-0.9436*
IPI00654731	Isoform 1 of Probable ATP-dependent RNA helicase DDX58	*0.5250*	*-0.9297*
IPI00022649	Isoform 1 of Solute carrier family 12 member 2	*0.5370*	*-0.8971*
IPI00103884	Ovarian cancer-associated gene 2 protein	*0.5401*	*-0.8888*
IPI00249304	Isoform 1 of Peroxisomal proliferator-activated receptor A-interacting complex 285 kDa protein	*0.5465*	*-0.8717*
IPI00514897	Brefeldin A-inhibited guanine nucleotide-exchange protein 3	*0.5484*	*-0.8668*
IPI00247871	Isoform 1 of Transcription elongation regulator 1	*0.5502*	*-0.8621*
IPI00167949	Interferon-induced GTP-binding protein Mx1	*0.5522*	*-0.8567*
IPI00873607	Isoform 1 of Thioredoxin-related transmembrane protein 2	*0.5548*	*-0.8499*
IPI00219871	U6 snRNA-associated Sm-like protein LSm8	*0.5549*	*-0.8497*
IPI00106687	Latexin	*0.5613*	*-0.8331*
IPI00294834	Aspartyl/asparaginyl beta-hydroxylase	*0.5736*	*-0.8019*
IPI00791049	HLA-B associated transcript 5, isoform CRA_b	*0.5743*	*-0.8000*
IPI00179473	Isoform 1 of Sequestosome-1	*0.5805*	*-0.7846*
IPI00293533	Nuclear pore glycoprotein p62	*0.5817*	*-0.7815*
IPI00184772	Putative uncharacterized protein DOCK6	*0.5832*	*-0.7780*
IPI00298793	Beta-mannosidase	*0.5837*	*-0.7768*
IPI00012545	Isoform TGN51 of Trans-Golgi network integral membrane protein 2	*0.5873*	*-0.7679*
IPI00061108	Isoform 1 of Ribosome-recycling factor, mitochondrial	*0.5889*	*-0.7638*
IPI00853099	Isoform 2 of Zinc finger transcription factor Trps1	*0.5965*	*-0.7454*
IPI00003818	Kynureninase	*0.5967*	*-0.7450*
IPI00004312	Isoform Long of Signal transducer and activator of transcription 2	*0.5983*	*-0.7411*
IPI00419979	p21 protein (Cdc42/Rac)-activated kinase 2	*0.5987*	*-0.7400*
IPI00008711	Wolframin	*0.6001*	*-0.7366*
IPI00409659	Ubiquilin-2	*0.6039*	*-0.7277*
IPI00305010	Isoform 1 of Calcineurin-like phosphoesterase domain-containing protein 1	*0.6051*	*-0.7247*
IPI00375631	Interferon-induced 17 kDa protein	*0.6059*	*-0.7229*
IPI00941977	ZYX protein (Fragment)	*0.6103*	*-0.7123*
IPI00005260	Isoform 1 of Proteasome activator complex subunit 4	*0.6105*	*-0.7119*
IPI00010187	Elongation of very long chain fatty acids protein 1	*0.6110*	*-0.7108*
IPI00009896	Epoxide hydrolase 1	*0.6177*	*-0.6950*
IPI00009982	Isoform 1 of Tudor and KH domain-containing protein	*0.6180*	*-0.6944*
IPI00013735	Isoform 1 of FAST kinase domain-containing protein 2	*0.6197*	*-0.6903*
IPI00100796	Charged multivesicular body protein 5	*0.6217*	*-0.6856*
IPI00002188	Brefeldin A-inhibited guanine nucleotide-exchange protein 1	*0.6220*	*-0.6850*
IPI00924788	arylacetamide deacetylase-like 1 isoform a	*0.6273*	*-0.6727*
IPI00647491	Isoform 1 of Mitochondrial ribonuclease P protein 3	*0.6291*	*-0.6686*
IPI00296907	Isoform 1 of Peroxisomal acyl-coenzyme A oxidase 1	*0.6310*	*-0.6643*
IPI00329572	Protein kinase C and casein kinase substrate in neurons protein 3	*0.6326*	*-0.6606*

IPI00215780	40S ribosomal protein S19	***0.6346***	***-0.6562***
IPI00296635	1,4-alpha-glucan-branching enzyme	***0.6355***	***-0.6540***
IPI00104050	Thyroid hormone receptor-associated protein 3	***0.6381***	***-0.6481***
IPI00414384	Isoform 1 of Hydroxysteroid dehydrogenase-like protein 2	***0.6395***	***-0.6449***
IPI00010207	Ubiquitin-fold modifier 1	***0.6435***	***-0.6360***
IPI00010400	1-phosphatidylinositol-4,5-bisphosphate phosphodiesterase beta-3	***0.6441***	***-0.6346***
IPI00023556	Isoform 1 of RNA polymerase II subunit A C-terminal domain phosphatase SSU72	***0.6447***	***-0.6333***
IPI00260715	Fus-like protein (Fragment)	***0.6463***	***-0.6297***
IPI00291783	Gem-associated protein 5	***0.6479***	***-0.6261***
IPI00334282	Protein FAM3C	***0.6489***	***-0.6238***
IPI00307257	Isoform 1 of TBC1 domain family member 9B	***0.6503***	***-0.6208***
IPI00291215	poly (ADP-ribose) polymerase family, member 14	***0.6529***	***-0.6151***
IPI00009225	Syntaxin-8	***0.6529***	***-0.6150***
IPI00102864	Hexokinase-2	***0.6530***	***-0.6149***
IPI00030098	Protein FAM50A	***0.6556***	***-0.6091***
IPI00470631	Isoform 1 of Ubiquinone biosynthesis protein COQ9, mitochondrial	***0.6571***	***-0.6058***
IPI00010440	Isoform 1 of HCLS1-associated protein X-1	***0.6590***	***-0.6016***
IPI00013930	Syntaxin-6	***0.6605***	***-0.5984***
IPI00220271	Alcohol dehydrogenase [NADP+]	***0.6608***	***-0.5977***
IPI00020719	Isoform 1 of Mitochondrial antiviral-signaling protein	***0.6618***	***-0.5956***
IPI00304163	C12orf10 protein	***0.6618***	***-0.5955***
IPI00337386	Isoform 2 of Pre-mRNA-processing factor 40 homolog A	***0.6649***	***-0.5889***
IPI00008986	Large neutral amino acids transporter small subunit 1	***0.6681***	***-0.5819***
IPI00398922	Protein phosphatase 1 regulatory subunit 14B	***0.6695***	***-0.5789***
IPI00030774	Isoform 4 of Tubulin-specific chaperone D	***0.6709***	***-0.5758***
IPI00152441	Isoform 1 of Minor histocompatibility antigen H13	***0.6714***	***-0.5748***
IPI00329410	Dolichyldiphosphatase 1	***0.6735***	***-0.5703***
IPI00307409	39S ribosomal protein L9, mitochondrial	***0.6765***	***-0.5639***
IPI00065063	Dehydrogenase/reductase SDR family member 1	***0.6773***	***-0.5622***
IPI00218163	Isoform 2 of Mucin-1	***0.6783***	***-0.5599***
IPI00025086	Cytochrome c oxidase subunit 5A, mitochondrial	***0.6814***	***-0.5534***
IPI00328911	E3 ubiquitin-protein ligase HECTD1	***0.6817***	***-0.5528***
IPI00306604	Integrin alpha-5	***0.6824***	***-0.5512***
IPI00012462	Eukaryotic translation initiation factor 2A	***0.6908***	***-0.5337***
IPI00329692	Isoform Long of Glycylpeptide N-tetradecanoyltransferase 1	***0.6927***	***-0.5297***
IPI00103654	Isoform 1 of Serine/threonine-protein phosphatase 4 regulatory subunit 2	***0.6934***	***-0.5282***
IPI00478657	G-rich sequence factor 1	***0.6937***	***-0.5277***
IPI00014311	cDNA FLJ56037, highly similar to Cullin-2	***0.6939***	***-0.5272***
IPI00219729	Mitochondrial 2-oxoglutarate/malate carrier protein	***0.6958***	***-0.5232***
IPI00003843	cDNA FLJ53324, highly similar to Tight junction protein ZO-2	***0.6963***	***-0.5223***
IPI00169342	Isoform 1 of RNA-binding protein 47	***0.6971***	***-0.5206***
IPI00926109	Isoform 2 of Putative ATP-dependent RNA helicase DHX30	***0.6999***	***-0.5148***
IPI00253036	Isoform I of CD99 antigen	***0.7032***	***-0.5081***
IPI00014068	Isoform 1 of Serine/threonine-protein kinase PAK 4	***0.7051***	***-0.5042***
IPI00910694	cDNA FLJ58598, highly similar to Homo sapiens NOL1/NOP2/Sun domain family, member 5 (NSUN5), transcript variant 1, mRNA	***0.7054***	***-0.5035***
IPI00873518	MAD1 mitotic arrest deficient-like 1	***0.7054***	***-0.5035***
IPI00016613	CSNK2A1 protein	***0.7065***	***-0.5012***
IPI00024976	Mitochondrial import receptor subunit TOM22 homolog	***0.7070***	***-0.5003***

Supplementary Table 3. Significance B test of KSR1 regulated proteins (SILAC data).

Protein IDs	Protein Descriptions	Log2 Ratio R10K8/R0K0	Log2 Ratio Sign B R10K8/R0K0
IPI00027505	Isoform 1 of Integrin alpha-V	-5.4019	0
IPI00789159	Ribosomal protein L23a, isoform CRA_a	-3.3446	1.37E-137
IPI00913961	18 kDa protein	-4.1856	5.36E-136
IPI00453473	Histone H4	-3.1097	1.72E-119
IPI00221089	40S ribosomal protein S13	-1.8471	2.56E-44
IPI00651622	2-5 oligoadenylate synthetase 1 p52 isoform	-1.7956	1.28E-26
IPI00291764	Histone H2A type 1	-1.3684	1.50E-25
IPI00651657	Isoform 1 of Kinase suppressor of Ras 1	2.1205	2.43E-15
IPI00012912	Carnitine O-palmitoyltransferase 2, mitochondrial	2.1068	3.60E-15
IPI00418471	Vimentin	-2.6024	2.37E-11
IPI00018300	Interferon-induced protein with tetratricopeptide repeats 1	-2.3413	2.17E-09
IPI00654731	Isoform 1 of Probable ATP-dependent RNA helicase DDX58	-0.9297	2.78E-08
IPI00022649	Isoform 1 of Solute carrier family 12 member 2	-0.8971	8.22E-08
IPI00215780	40S ribosomal protein S19	-0.6562	1.84E-07
IPI00030781	Isoform Alpha of Signal transducer and activator of transcription 1-alpha/beta	1.345	2.57E-07
IPI00167949	Interferon-induced GTP-binding protein Mx1	-0.8567	3.01E-07
IPI00106687	Latexin	-0.8331	6.25E-07
IPI00002441	Syndecan-1	-1.1992	1.00E-06
IPI00002606	Isoform 1 of Adseverin	0.864	1.02E-06
IPI00216219	Isoform Long of Tight junction protein ZO-1	-1.8256	4.08E-06
IPI00419979	p21 protein (Cdc42/Rac)-activated kinase 2	-0.74	9.31E-06
IPI00375631	Interferon-induced 17 kDa protein	-0.7229	1.48E-05
IPI00011200	D-3-phosphoglycerate dehydrogenase	0.7297	3.31E-05
IPI00015141	Creatine kinase S-type, mitochondrial	-1.6441	3.75E-05
IPI00787853	Inositol monophosphatase 3	-0.4843	7.77E-05
IPI00008454	DnaJ homolog subfamily B member 11	-0.4786	9.24E-05
IPI00260715	Fus-like protein (Fragment)	-0.6297	0.000156903
IPI00011229	Cathepsin D	-0.454	0.000192336
IPI00304082	Isochorismatase domain-containing protein 1	0.6534	0.000229765
IPI00215637	ATP-dependent RNA helicase DDX3X	-0.4458	0.000243857
IPI00183110	Isoform 1 of Paternally-expressed gene 3 protein	0.6416	0.000305972
IPI00657888	Isoform 2 of Mannose-1-phosphate guanyltransferase alpha	-1.4349	0.000365313
IPI00878252	Isoform 1 of General transcription factor 3C polypeptide 2	-1.4197	0.000426105
IPI00008986	Large neutral amino acids transporter small subunit 1	-0.5819	0.000470449
IPI00297910	Tumor-associated calcium signal transducer 2	0.6071	0.000628294
IPI00554481	Isoform 4 of 4F2 cell-surface antigen heavy chain	-0.4038	0.000779341
IPI00025086	Cytochrome c oxidase subunit 5A, mitochondrial	-0.5534	0.000873456
IPI00797038	mitochondrial phosphoenolpyruvate carboxykinase 2 isoform 1 precursor	0.5932	0.00092276

Supplementary Table 4. SILAC KSR1-upregulated phosphorylated proteins (– log_2 >0.15 fold).

Protein IDs	Protein Descriptions	Normalised R10K8/R0K0	Log_2 R10K8/R0K0
IPI00418169	Isoform 2 of Annexin A2	2.933	1.552
IPI00376756	similar to high mobility group box 3	1.886	0.916
IPI00152409	Anterior gradient protein 3 homolog	1.616	0.692
IPI00021405	Isoform A of Lamin-A/C	1.454	0.540
IPI00900293	filamin B isoform 1	1.452	0.538
IPI00554788	Keratin, type I cytoskeletal 18	1.450	0.536
IPI00026530	Protein ERGIC-53	1.435	0.521
IPI00216319	14-3-3 protein eta	1.434	0.520
IPI00013214	MCM3 minichromosome maintenance deficient 3 (S. cerevisiae), isoform CRA_b	1.426	0.512
IPI00026215	Flap endonuclease 1	1.421	0.507
IPI00473136	Isoform 2 of Catenin alpha-1	1.410	0.496
IPI00394926	DNA polymerase delta subunit 3	1.387	0.472
IPI00657752	Putative uncharacterized protein CD81	1.376	0.461
IPI00017451	Splicing factor 3 subunit 1	1.369	0.453
IPI00843975	Ezrin	1.356	0.440
IPI00164672	Putative uncharacterized protein DCP1A	1.353	0.436
IPI00470502	Isoform 2 of Inorganic pyrophosphatase 2, mitochondrial	1.344	0.426
IPI00019502	Isoform 1 of Myosin-9	1.306	0.385
IPI00020017	Adipose most abundant gene transcript 2 protein	1.300	0.378
IPI00217405	Isoform 1 of E3 ubiquitin-protein ligase UBR1	1.292	0.370
IPI00883857	Isoform Long of Heterogeneous nuclear ribonucleoprotein U	1.282	0.358
IPI00299507	Condensin complex subunit 2	1.270	0.344
IPI00886784	similar to hCG1991922	1.268	0.343
IPI00746934	Isoform 2 of E3 ubiquitin-protein ligase UBR4	1.265	0.340
IPI00294426	Isoform Long of TATA-binding protein-associated factor 2N	1.265	0.339
IPI00303439	cDNA FLJ13963 fis, clone Y79AA1001299, highly similar to Homo sapiens integrase interactor 1b protein	1.265	0.339
IPI00021812	Neuroblast differentiation-associated protein AHNAK	1.260	0.334
IPI00019329	Dynein light chain 1, cytoplasmic	1.259	0.332
IPI00015029	Prostaglandin E synthase 3	1.256	0.329
IPI00294065	Isoform 1 of Golgin subfamily A member 5	1.255	0.328
IPI00872028	NUMA1 variant protein (Fragment)	1.254	0.327
IPI00062037	Dynein light chain 2, cytoplasmic	1.252	0.324
IPI00004860	Isoform Complexed of Arginyl-tRNA synthetase, cytoplasmic	1.247	0.318
IPI00465248	Isoform alpha-enolase of Alpha-enolase	1.246	0.318
IPI00022002	cDNA FLJ54536, highly similar to Mitochondrial 28S ribosomal protein S27	1.246	0.317
IPI00069084	Isoform 1 of Transformation/transcription domain-associated protein	1.240	0.310
IPI00643591	cDNA FLJ46199 fis, clone TESTI4007965, highly similar to AP-1 complex subunit gamma-1	1.235	0.304
IPI00033130	SUMO-activating enzyme subunit 1	1.229	0.297
IPI00027834	Heterogeneous nuclear ribonucleoprotein L	1.227	0.295
IPI00852968	SNARE Vti1a-beta protein	1.216	0.282
IPI00844578	ATP-dependent RNA helicase A	1.213	0.278
IPI00001159	Translational activator GCN1	1.210	0.275
IPI00385652	Isoform 1 of Serine/threonine-protein kinase tousled-like 2	1.206	0.270
IPI00007074	Tyrosyl-tRNA synthetase, cytoplasmic	1.202	0.265
IPI00032780	Intersex-like	1.200	0.263
IPI00009342	Ras GTPase-activating-like protein IQGAP1	1.198	0.261
IPI00018349	DNA replication licensing factor MCM4	1.196	0.258
IPI00007928	Pre-mRNA-processing-splicing factor 8	1.195	0.256
IPI00021263	14-3-3 protein zeta/delta	1.193	0.255
IPI00013933	Isoform DPI of Desmoplakin	1.191	0.252
IPI00008274	Isoform 1 of Adenylyl cyclase-associated protein 1	1.190	0.251
IPI00607584	Isoform 2 of Myb-binding protein 1A	1.185	0.245
IPI00031627	DNA-directed RNA polymerase II subunit RPB1	1.183	0.243
IPI00165230	Isoform 1 of DAZ-associated protein 1	1.183	0.242
IPI00072534	Isoform 1 of Protein unc-45 homolog A	1.183	0.242
IPI00884061	hypothetical protein LOC552889	1.182	0.242
IPI00235412	cDNA FLJ56381, highly similar to Dynamin-1-like protein	1.181	0.240
IPI00414717	Isoform 2 of Golgi apparatus protein 1	1.177	0.235
IPI00007021	Mediator of RNA polymerase II transcription subunit 31	1.174	0.232

IPI00096066	Succinyl-CoA ligase [GDP-forming] subunit beta, mitochondrial	**1.174**	**0.231**
IPI00289819	Cation-independent mannose-6-phosphate receptor	**1.169**	**0.225**
IPI00021440	Actin, cytoplasmic 2	**1.168**	**0.224**
IPI00942520	cDNA FLJ55610, highly similar to Protein arginine N-methyltransferase 1	**1.166**	**0.222**
IPI00419249	Isoform 1 of Proteasome subunit alpha type-3	**1.166**	**0.222**
IPI00000816	14-3-3 protein epsilon	**1.160**	**0.215**
IPI00024368	Isoform Long of Probable phospholipid-transporting ATPase IIA	**1.155**	**0.208**
IPI00394668	Isoform 4 of Double-stranded RNA-specific adenosine deaminase	**1.151**	**0.203**
IPI00409684	Isoform 2 of Nck-associated protein 1	**1.150**	**0.201**
IPI00215637	ATP-dependent RNA helicase DDX3X	**1.146**	**0.197**
IPI00101374	cDNA FLJ61658, highly similar to Transmembrane 9 superfamily protein member 1	**1.146**	**0.197**
IPI00929344	phosphoribosylformylglycinamidine synthase	**1.145**	**0.196**
IPI00306400	Kinesin-like protein KIFC1	**1.145**	**0.195**
IPI00307155	Rho-associated protein kinase 2	**1.145**	**0.195**
IPI00018098	Isoform 1 of Pre-mRNA-splicing factor 38B	**1.142**	**0.192**
IPI00916768	21 kDa protein	**1.141**	**0.190**
IPI00216318	Isoform Long of 14-3-3 protein beta/alpha	**1.132**	**0.179**
IPI00028055	Transmembrane emp24 domain-containing protein 10	**1.129**	**0.176**
IPI00440493	ATP synthase subunit alpha, mitochondrial	**1.126**	**0.172**
IPI00027107	Tu translation elongation factor, mitochondrial precursor	**1.126**	**0.171**
IPI00022020	Type II inositol-3,4-bisphosphate 4-phosphatase	**1.121**	**0.165**
IPI00215998	CD63 antigen	**1.120**	**0.164**
IPI00033600	Isoform 1 of Protein phosphatase 1 regulatory subunit 7	**1.120**	**0.163**
IPI00024466	Isoform 1 of UDP-glucose:glycoprotein glucosyltransferase 1	**1.118**	**0.161**
IPI00021174	Isoform Long of ADP-ribosylation factor-binding protein GGA3	**1.117**	**0.160**
IPI00034049	Isoform 1 of Regulator of nonsense transcripts 1	**1.115**	**0.157**
IPI00008529	60S acidic ribosomal protein P2	**1.114**	**0.156**
IPI00438229	Isoform 1 of Transcription intermediary factor 1-beta	**1.114**	**0.156**
IPI00719643	Putative uncharacterized protein SETX	**1.113**	**0.155**
IPI00015602	Mitochondrial import receptor subunit TOM70	**1.110**	**0.150**

Supplementary Table 5. SILAC KSR1-downregulated phosphorylated proteins (– log_2 <0.15 fold).

Protein IDs	Protein Descriptions	Normalised R10K8/R0K0	Log_2 R10K8/R0K0
IPI00022990	Statherin	0.059	-4.072
IPI00004573	Polymeric immunoglobulin receptor	0.155	-2.692
IPI00217049	Isoform p71 of 2-5-oligoadenylate synthetase 2	0.250	-1.999
IPI00719752	Isoform 2 of Eukaryotic translation initiation factor 3 subunit B	0.509	-0.973
IPI00026320	E3 ubiquitin-protein ligase UBR5	0.545	-0.875
IPI00843759	Putative uncharacterized protein YTHDF1	0.553	-0.854
IPI00333410	Isoform 1 of Ubiquitin-conjugating enzyme E2 Q1	0.565	-0.823
IPI00012268	26S proteasome non-ATPase regulatory subunit 2	0.595	-0.748
IPI00797230	32 kDa protein	0.601	-0.734
IPI00456363	Isoform 3 of Ataxin-2-like protein	0.617	-0.696
IPI00016608	Transmembrane emp24 domain-containing protein 2	0.633	-0.660
IPI00010951	epiplakin 1	0.634	-0.657
IPI00002441	Syndecan-1	0.651	-0.620
IPI00027230	Endoplasmin	0.668	-0.582
IPI00797384	Isoform 4 of La-related protein 4	0.671	-0.577
IPI00328257	Isoform A of AP-1 complex subunit beta-1	0.675	-0.567
IPI00000728	Isoform 1 of Ubiquitin carboxyl-terminal hydrolase 15	0.678	-0.561
IPI00376394	Sulfhydryl oxidase 2	0.683	-0.549
IPI00854642	Isoform 1 of Sister chromatid cohesion protein PDS5 homolog A	0.687	-0.542
IPI00011229	Cathepsin D	0.687	-0.541
IPI00847793	Dermcidin isoform 2	0.688	-0.539
IPI00922415	cDNA FLJ51825, highly similar to Single-stranded DNA-binding protein, mitochondrial	0.693	-0.530
IPI00291783	Gem-associated protein 5	0.693	-0.529
IPI00307572	Transmembrane protein 165	0.696	-0.524
IPI00219774	cAMP-dependent protein kinase type II-alpha regulatory subunit	0.701	-0.512
IPI00220301	Peroxiredoxin-6	0.707	-0.500
IPI00925413	EIF4G1 protein	0.709	-0.496
IPI00385267	Signal recognition particle receptor subunit alpha	0.717	-0.480
IPI00607554	Isoform 1 of Ubiquitin carboxyl-terminal hydrolase 47	0.719	-0.476
IPI00217354	Isoform 2 of ADP-ribosylation factor GTPase-activating protein 1	0.727	-0.460
IPI00219077	Isoform 1 of Leukotriene A-4 hydrolase	0.730	-0.454
IPI00795906	MHC class I antigen heavy chain	0.730	-0.453
IPI00016095	Transcription termination factor, mitochondrial	0.734	-0.446
IPI00032491	Inner nuclear membrane protein Man1	0.735	-0.445
IPI00026991	Polypeptide N-acetylgalactosaminyltransferase 6	0.739	-0.436
IPI00011609	Isoform II of Ubiquitin-protein ligase E3A	0.741	-0.432
IPI00182757	Isoform 1 of Protein KIAA1967	0.748	-0.419
IPI00256861	Isoform 2 of Microtubule-actin cross-linking factor 1, isoforms 1/2/3/5	0.749	-0.417
IPI00216044	Isoform 1 of RNA-binding protein Raly	0.750	-0.414
IPI00031812	Nuclease-sensitive element-binding protein 1	0.757	-0.402
IPI00456969	Cytoplasmic dynein 1 heavy chain 1	0.762	-0.393
IPI00030911	Vesicle-associated membrane protein 8	0.765	-0.387
IPI00002255	Isoform 1 of Lipopolysaccharide-responsive and beige-like anchor protein	0.765	-0.386
IPI00003843	cDNA FLJ53324, highly similar to Tight junction protein ZO-2	0.770	-0.377
IPI00254162	cDNA FLJ55936, highly similar to Polypyrimidine tract-binding protein 2	0.772	-0.374
IPI00953703	Putative uncharacterized protein GOLGA5	0.773	-0.371
IPI00007426	PRA1 family protein 3	0.777	-0.365
IPI00031420	UDP-glucose 6-dehydrogenase	0.777	-0.364
IPI00010252	Isoform Alpha of E3 ubiquitin-protein ligase TRIM33	0.781	-0.356
IPI00024993	Enoyl-CoA hydratase, mitochondrial	0.784	-0.352
IPI00008524	Isoform 1 of Polyadenylate-binding protein 1	0.788	-0.344
IPI00024976	Mitochondrial import receptor subunit TOM22 homolog	0.791	-0.339
IPI00295252	Isoform 1 of Phosphatidylinositol 3,4,5-trisphosphate-dependent Rac exchanger 1 protein	0.797	-0.327
IPI00019600	Ubiquitin-conjugating enzyme E2 variant 2	0.798	-0.326
IPI00796337	poly(rC) binding protein 2 isoform a	0.798	-0.325
IPI00784614	septin 9 isoform a	0.800	-0.323
IPI00217540	Isoform 2 of Lysine-specific histone demethylase 1	0.803	-0.317
IPI00413108	33 kDa protein	0.804	-0.315
IPI00742743	Isoform 2 of Tumor suppressor p53-binding protein 1	0.813	-0.298

IPI00036742	Isoform 1 of Protein virilizer homolog	**0.814**	**-0.297**
IPI00465152	Transcription factor Sp1	**0.816**	**-0.293**
IPI00020985	Histone acetyltransferase p300	**0.818**	**-0.289**
IPI00815944	Isoform 3 of Treacle protein	**0.822**	**-0.283**
IPI00029629	E3 ubiquitin/ISG15 ligase TRIM25	**0.824**	**-0.280**
IPI00218782	cDNA FLJ60094, highly similar to F-actin capping protein subunit beta	**0.825**	**-0.277**
IPI00026781	Fatty acid synthase	**0.828**	**-0.273**
IPI00021048	Isoform 1 of Myoferlin	**0.829**	**-0.270**
IPI00302927	T-complex protein 1 subunit delta	**0.832**	**-0.265**
IPI00784414	Isoform 1 of Signal transducer and activator of transcription 3	**0.834**	**-0.263**
IPI00479786	KH-type splicing regulatory protein	**0.835**	**-0.260**
IPI00029012	Eukaryotic translation initiation factor 3 subunit A	**0.845**	**-0.243**
IPI00386448	Isoform 1 of Transcription factor p65	**0.848**	**-0.239**
IPI00514983	Heat shock 105kDa/110kDa protein 1, isoform CRA_b	**0.850**	**-0.234**
IPI00013272	Isoform 1 of Golgin subfamily A member 4	**0.850**	**-0.234**
IPI00016342	Ras-related protein Rab-7a	**0.857**	**-0.223**
IPI00396378	Isoform B1 of Heterogeneous nuclear ribonucleoproteins A2/B1	**0.857**	**-0.223**
IPI00333541	Isoform 1 of Filamin-A	**0.858**	**-0.221**
IPI00186290	Elongation factor 2	**0.861**	**-0.216**
IPI00083708	Isoform 7 of BAT2 domain-containing protein 1	**0.861**	**-0.215**
IPI00032635	Isoform 1 of Protein LSM14 homolog B	**0.863**	**-0.213**
IPI00216746	Isoform 2 of Heterogeneous nuclear ribonucleoprotein K	**0.863**	**-0.213**
IPI00409717	Isoform 2 of Eukaryotic initiation factor 4A-II	**0.863**	**-0.213**
IPI00915260	Isoform 1 of Cyclin-K	**0.866**	**-0.208**
IPI00019380	Nuclear cap-binding protein subunit 1	**0.867**	**-0.205**
IPI00022228	Vigilin	**0.869**	**-0.202**
IPI00514856	Isoform 1 of Ubiquitin-associated protein 2-like	**0.870**	**-0.201**
IPI00018813	Isoform 2 of COP9 signalosome complex subunit 2	**0.871**	**-0.200**
IPI00412343	Isoform 6 of Fragile X mental retardation 1 protein	**0.871**	**-0.199**
IPI00005737	Isoform 1 of Surfeit locus protein 4	**0.871**	**-0.199**
IPI00293735	Elongator complex protein 1	**0.872**	**-0.198**
IPI00383581	cDNA FLJ61290, highly similar to Neutral alpha-glucosidase AB	**0.874**	**-0.195**
IPI00031819	UPF0139 membrane protein C19orf56	**0.874**	**-0.194**
IPI00215914	ADP-ribosylation factor 1	**0.878**	**-0.188**
IPI00473014	Destrin	**0.881**	**-0.183**
IPI00294879	Ran GTPase-activating protein 1	**0.884**	**-0.178**
IPI00178150	Isoform 1 of Chromosome-associated kinesin KIF4A	**0.889**	**-0.170**
IPI00942869	Isoform 1ABC of Catenin delta-1	**0.898**	**-0.156**
IPI00020984	cDNA FLJ55574, highly similar to Calnexin	**0.898**	**-0.156**
IPI00219678	Eukaryotic translation initiation factor 2 subunit 1	**0.898**	**-0.155**
IPI00409671	Isoform 1 of ATP-dependent RNA helicase DDX42	**0.899**	**-0.154**
IPI00010740	Isoform Long of Splicing factor, proline- and glutamine-rich	**0.900**	**-0.151**
IPI00026182	F-actin-capping protein subunit alpha-2	**0.901**	**-0.151**